

J 20 419 F



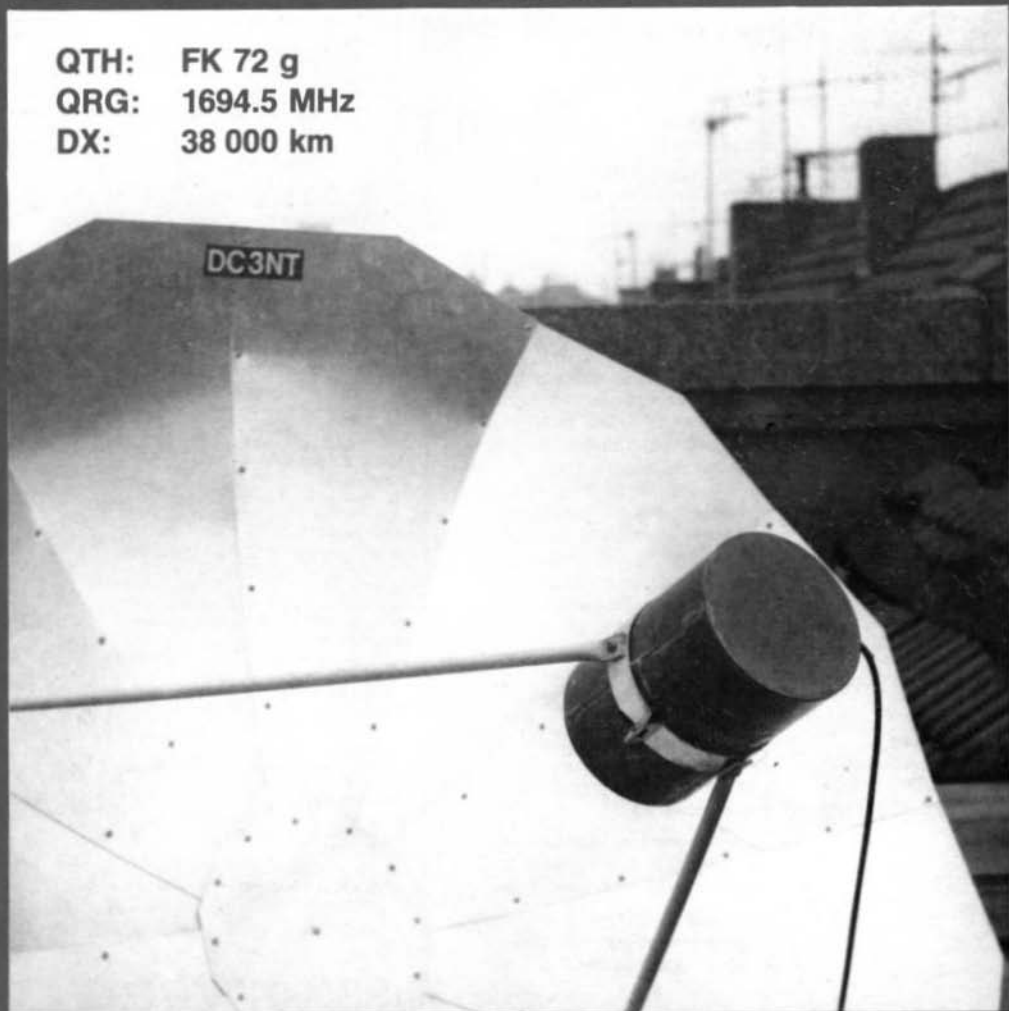
*A Publication
for the Radio-Amateur
Especially Covering VHF,
UHF and Microwaves*

VHF

communications

Volume No. 11 · Autumn · 3/1979 · DM 5.00

QTH: FK 72 g
QRG: 1694.5 MHz
DX: 38 000 km





VHF communications

A Publication for the Radio Amateur
Especially Covering VHF, UHF, and Microwaves

Volume No. 11 - Autumn - Edition 3/1979

Published by:

Verlag UKW-BERICHTE,
Terry Bittan
Jahnstrasse 14
D-8523 BAIERSDORF
Fed. Rep. of Germany
Telephones (09133) 855, 856.

Publisher:

Terry Bittan, DJ 0 BQ

Editors:

Terry D. Bittan, G 3 JVQ / DJ 0 BQ,
responsible for the text
Robert E. Lentz, DL 3 WR,
responsible for the technical
contents

**Advertising
manager:**

Terry Bittan

**VHF COMMU-
NICATIONS**

The international edition of the German publication UKW-BERICHTE, is a quarterly amateur radio magazine especially catering for the VHF/UHF/SHF technology. It is published in Spring, Summer, Autumn, and Winter. The subscription price is DM 20.00 or national equivalent per year. Individual copies are available at DM 5.50 or equivalent, each. Subscriptions, orders of individual copies, purchase of PC-boards and advertised special components, advertisements and contributions to the magazine should be addressed to the national representative.

© Verlag
UKW-BERICHTE
1981

All rights reserved. Reprints, translations, or extracts only with the written approval of the publisher.

Printed in the Fed. Rep. of Germany by R. Reichenbach KG, Krelingstr. 39 · 8500 Nuernberg.

We would be grateful if you would address your orders and queries to your representative.

VERTRETUNGEN · REPRESENTATIVES:

Austria

Verlag UKW-BERICHTE, Terry D. Bittan
POB 80, D-8523 Baiersdorf/W Germany
Creditanstalt Bankverein, WIEN Kto. 17-90.599.
PSchKto WIEN 1.169.146

Australia

W I A, P.O. Box 300, South Caulfield, 3162 VIC, Phone 5285962

Belgium

HAM INTERNATIONAL, Brusselsesteenweg 428, B-9218 GENT,
PCR 000-1014257 CCP, Tel. 00-32-91-312111

Denmark

Halskov Electronic, OZ7LX, Sigersted gamle Skole,
DK-4100 RINGSTED, Telf. 03-616162, Giro 7 29 68 00

France

Christiane Michel, F 5 SM, SM Electronic,
20 bis, Avenue des Clairons, F-89000 AUXERRE
Tel. (86) 46 96 59

Finland

Erkki Hohenthal, SF-31400 SOMERO
Joensuuentie 6, Tel. 924-46311

Holland

MECOM, PA 0 AER, Postbus 40, Noordwolderweg 12,
NL-9780 AA BEDUM, Tel. 05900-14390
Postgiro 3986163

Israel

Z. Pomer, 4X4KT, PO Box 222, K. MOZKIN 26114
Tel. 00972-4714078

Italy

Franco Armenghi, I 4 LCK, Via Sigonio 2,
I-40137 BOLOGNA, Tel. (051) 34 56 97

Luxembourg

TELECO, Jos. Faber, LX 1 DE, 5-9, Rue de la fontaine,
ESCH-SUR-ALZETTE, Tel. 53752

New Zealand

E. M. Zimmermann, ZL 1 AGQ, PO Box 31-261
Milford, AUCKLAND 9, Phone 492-744

Norway

Henning Thieg, LA 4 YG, Postboks 70,
N-1324 LYSAKER, Postgirokonto 3 16 00 09

South Africa

SA Radio Publications, PO Box 2232, JOHANNES-
BURG 2000, Telephone 011-3378472

Spain + Portugal

Julio A. Prieto Alonso, EA 4 CJ, MADRID-15,
Donoso Cortés 58 5°-B, Tel. 243.83.84

Sweden

Carl-Oscar Biese, SMeHVL, Guterbacken 12 B
S-17239 SUNDBYBERG, Tel. 08-29 63 22

Switzerland

Terry Bittan, Schweiz, Kreditanstalt ZÜRICH,
Kto. 469.253-41, PSchKto ZÜRICH 80-54.849

USA

UV COMMS, K3BRS
PO Box 432, LANHAM, MD 20706
Tel. 301-459-4924

ISSN 0177-7505

**A PUBLICATION FOR THE RADIO AMATEUR
ESPECIALLY COVERING VHF, UHF AND MICROWAVES
VOLUME No. 11 AUTUMN EDITION 3/1979**

R. Tellert DC 3 NT	A System for Reception and Display of METEOSAT Images	130 - 140
O. Frosinn DF 7 QF	A Frequency Doubler for the 13 cm Band with 6 W Output Power	141 - 143
R. Heidemann DC 3 QS	SSB Transmit Mixers for the SHF Bands Part 2: The 9 cm Band	144 - 150
R. Heidemann DC 3 QS	A Simple Radiator for 3 cm Parabolic Dishes	151 - 153
G. Hoch DL 6 WU	Optimum Spacings of Directional Antennas	154 - 161
J. Becker DJ 8 IL	A 20 W Power Amplifier with Integrated PA-Module for FM Transceivers on the 2 m Band	162 - 169
A. Meier DC 7 MA	Quadrature Demodulators	170 - 173
B. Neubig DK 1 AG	Design of Crystal Oscillator Circuits	174 - 190
Editor	Notes and Modifications	190 - 191

PARABOLIC DISHES are rather rare, and difficult to obtain. For this reason we have manufactured a few types of dishes for SHF and microwave use. A kit for a 1.2 m dish and radiator are given in the price list. This dish is suitable up to about 3-4 GHz. We have also manufactured a dish for 10 GHz with following specifications:

Material: Pure aluminium, 1.2 mm thick ● Diameter: 450 mm ● Gain: approximately 30 dB ● Weight: 500 g ● Focal distance: $f = 200$ mm ● Supplied without radiator. Please ask your representative for price.

A SYSTEM FOR RECEPTION AND DISPLAY OF METEOSAT IMAGES

Part 1

by R. Tellert, DC 3 NT

The image acquisition and transmission system of the European weather satellite METEOSAT was described in detail in (1) and (2). The author developed and constructed a system that roughly corresponds to that given in Figure 10 in (2). This system is to be described in this and further editions of VHF COMMUNICATIONS for construction.

Part 1 of this article is to give a brief description of the overall system and is to describe a home-made parabolic antenna for 1691/1694.5 MHz having a diameter of 1.2 m.

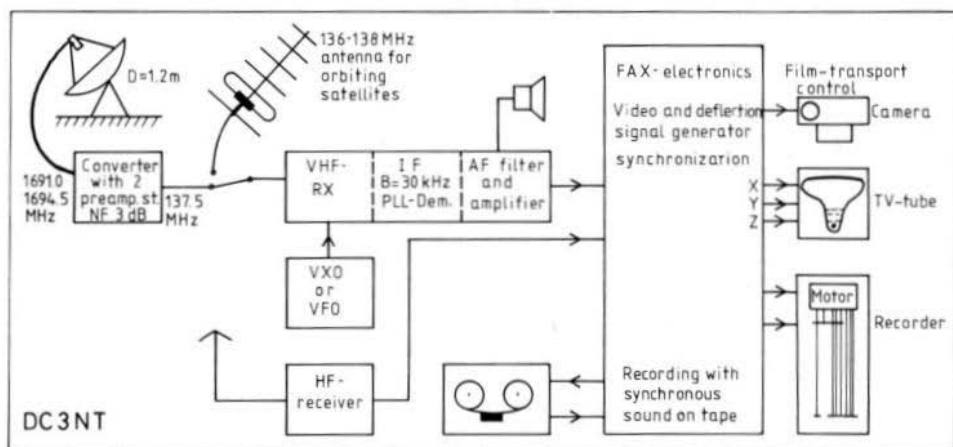


Fig. 1: Modules of the METEOSAT reception at DC 3 NT

1. CONCEPT

The following modules are used to obtain noise-free images from the METEOSAT-APT transmissions:

1. A 1.2 m parabolic dish with tubular radiator, and 1.5 m coaxial cable.
2. METEOSAT converter 1691/1694.5 MHz to 137.5 MHz with BFR 14 B preamplifier.
3. A 137.5 MHz FM receiver, tuneable ± 25 kHz, double conversion to 10.7 MHz and 455 kHz IFs with subsequent PLL-demodulator and AF bandpass filter, as well as input/output for recording in conjunction with a tape recorder.
4. Image recording using a 44 cm TV-tube with signal processing for modulation of the cathode beam, deflection control, and synchronization, as well as the required HT-supply.

5. A 25 mm camera with motorized film transport that can be controlled from the receiver, as well as electronic switching at the end of the image.
6. Furthermore, alternately, an electro-mechanical facsimile recorder that generates images on metalized paper.

The previously mentioned components of the image reception system of the author are given in **Figure 1**. The system is completed by addition of a shortwave receiver for reception of weather map transmissions, and a tape recorder for storing the received images. Since the construction cannot be described in one edition, and since the preparation of the manuscripts is time-consuming, and must therefore be spread over several editions, the overall system is to be described briefly as follows:

1.1. The Video Reception System at DC 3 NT

A home-made parabolic dish of 1.2 m diameter is used as antenna for the 1691/1694.5 MHz METEOSAT transmissions. The parabolic dish is made from 12 segments and a round disk at the center. The individual segments are cut from 1 mm aluminium plate and are drilled so that a parabolic shape will result when the individual segments are screwed or rivetted together. The only critical point is the calculation and exact drilling of the holes according to a parabolic characteristic. Since a screw or rivet is only placed every 10 cm, a slightly rippled parabolic dish will result after completion that has overlapping metal edges. However, the inaccuracies are without noticeable influence at a wavelength of 17.7 cm.

A tubular radiator as described in (3) was recalculated for 1693 MHz and is used for illuminating the dish. Since METEOSAT signals have been found to arrive virtually horizontally polarized, the radiator element in the tube is mounted in a horizontal direction. The tubular radiator is mounted at the focal point using a tripod. The parabolic dish is fixed to an adjustable mount. The radiator is connected to the converter using N-connectors and a maximum of 2 m coaxial cable (RG-213). It should be mentioned that measures should be taken to ensure that no humidity or condensation can get into the coaxial connections, as well as to ensure that the converter is not subjected to great temperature variations and other effects that can cause condensed water in the converter.

The converter is constructed using resonant chambers; it comprises two RF preamplifier stages: the first stage is equipped with a transistor type BFR 14 B (Siemens). Noise-free images were only possible after using this transistor, what was not possible when using a BFT 65 or BFR 34 A.

A transistor type BFT 65 is used in the second preamplifier stage and in the active mixer. The intermediate frequency of 137.5 MHz is amplified in a DG-MOSFET and a hybrid wideband amplifier OM 335 so that it is even possible for a very long cable to be used between the converter and the VHF receiver. The only special feature of the oscillator chain of the converter is that the last tripler uses a cheap switching diode type 1 N 4148. It is driven with approximately 10 mW at 517.8/519 MHz and provides sufficient power for conversion at 1553.5/1557.0 MHz.

The 137.5 MHz FM receiver is equipped with a low-noise DG-MOSFET BF 900 in the input. The input signal is firstly converted to 10.7 MHz where a crystal filter having a bandwidth of 30 kHz provides the main selectivity. The required local oscillator signal of 126.8 MHz is pro-

vided either by a variable crystal oscillator (VXO) or by a variable LC-oscillator with automatic frequency control (AFC) and scanning circuit to find the signal after transmission pauses. A fixed crystal-controlled oscillator cannot be used at this position, since the crystal-controlled frequencies in the satellite itself, and in the converter can vary due to a number of effects. For this reason, it is necessary to provide a tuning possibility somewhere in the system; a variation of ± 25 kHz is sufficient.

In order to also be able to record the APT transmissions of the weather satellites having a polar orbit, the FM receiver can be connected to a 136 to 138 MHz antenna and the mixer fed with a variable oscillator (Superhet VFO, PLL-oscillator, synthesizer, etc.), that is variable between 125.3 and 127.3 MHz.

The second IF-amplifier at 455 kHz is equipped with low-noise DG-MOSFETs and resonant circuits between stages in order to ensure that no wideband noise is generated. The following PLL-demodulator is also designed with this in mind. It is constructed in the form of a tracking filter, and possesses a lowpass filter in its control loop, whose cut-off frequency is lower than the IF bandwidth.

The receiver circuit is then completed using an audio low-pass filter with a cut-off frequency of 4 kHz, an audio high-pass filter of 800 Hz, as well as an integrated audio amplifier with squelch. This allows one to monitor the 2400 Hz tone that is modulated with the video signal.

The images can be recorded using this system in two ways: The first method is new when recording images having grey steps. The images are recorded on metalized paper, which is used in inexpensive plotters in the periphery equipment for micro-processors. The second method was described in (2): The image is traced on a TV-tube and photographed by a camera.

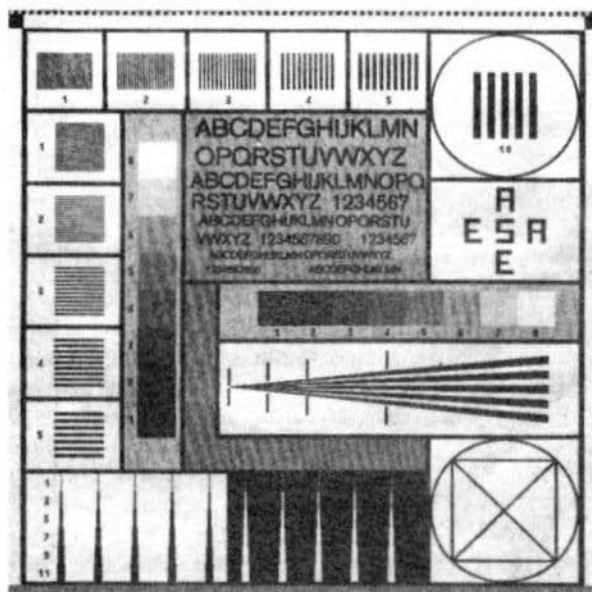


Fig. 2: An ESA test pattern received via METEOSAT using the FAX-machine

Figure 2 gives an example of the quality of the electro-mechanical image recording module (FAX-machine) in the form of the ESA-test pattern transmitted via METEOSAT. The original dimensions are 120 mm x 120 mm and it does not exhibit any geometric distortion. The resolution is also excellent; the disadvantage of this system is in the low contrast between the grey steps. The mechanical construction of this unit is not too extensive. The metalized paper is in the form of a roll on a metal drum which is driven by a synchronous motor from a crystal-controlled source. The needle is mounted on a slide which moves horizontally along the drum. If a voltage (video signal) is present between the pin and the drum, the metalized surface (aluminium) on the paper will be burnt away, and the black paper will be visible. However, the deep black of photographic paper will not be achieved. The grey levels are obtained using dots (pulse widths-modulation).

Figure 3 shows a photograph of the author's FAX-machine, which looks similar to Edison's first gramophone, and the operation is very similar.

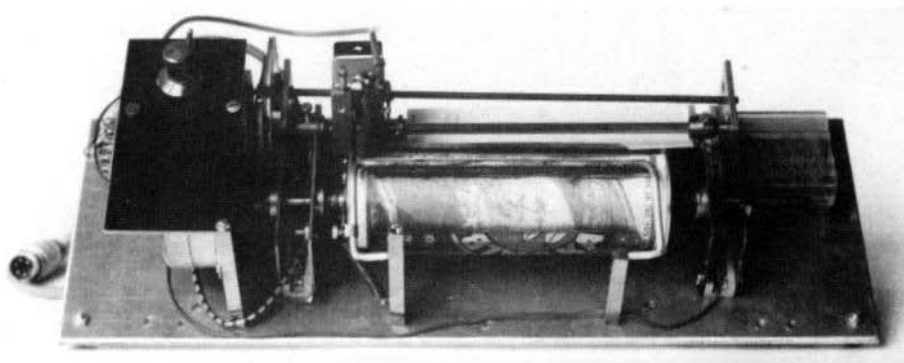


Fig. 3: Photograph of the author's prototype FAX-machine

The images shown in **Figure 4** were made, using a home-made camera, by photographing the image traced on a TV-tube. Shown are a series of images transmitted on February 16, 1979. The individual images have been combined using an enlarger. The narrow white and black lines between the images are caused by inaccuracies of the mask; they have nothing to do with the actual video recording system. The camera does not have a shutter, but is provided with a motor for transporting the film.

It switches itself off automatically after the film has been transported 25 mm. This allows 49 to 50 images of 23 mm x 23 mm to be photographed on one film. A suitable lens was found in the author's camera box.

Since 15 images per hour are transmitted via METEOSAT, the described system can record all images transmitted by METEOSAT for a period of 3 hours. If the operator cannot be present during this period, it is possible for the system to be controlled by a clock, which has been programmed for the most interesting periods according to the dissemination schedule.

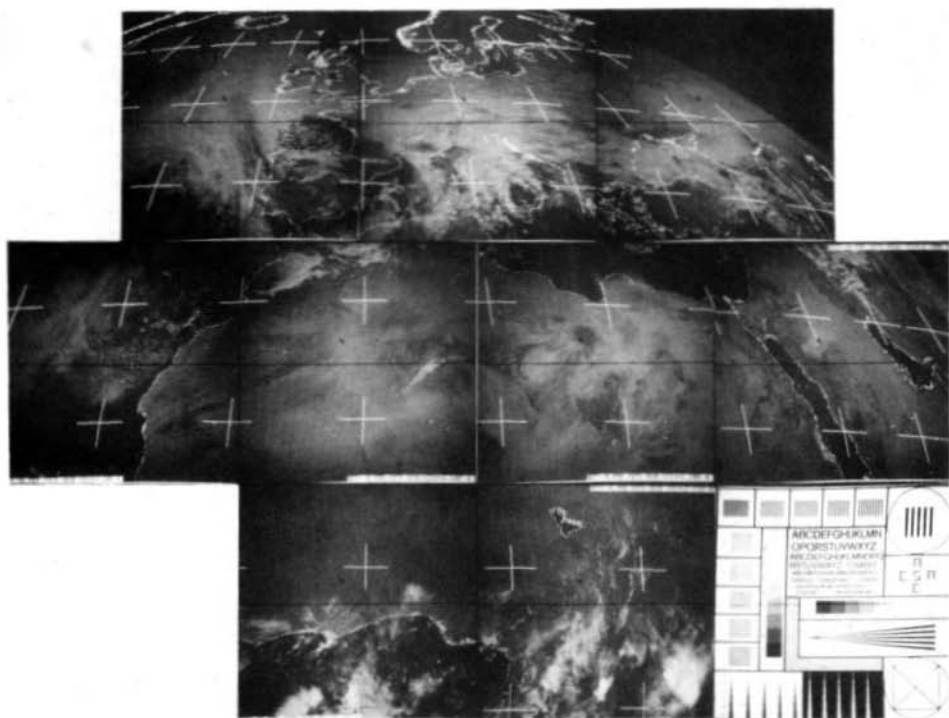


Fig. 4: A sequence of METEOSAT images recorded on February 16, 1979, and combined with the aid of an enlarger

Both methods of image acquisition have their advantages and disadvantages which are to be compared in the following table:

Characteristic	Image recording on	
	Metalized paper	TV-tube/camera
Cost per image	+	-
Contrast (grey steps)	-	+
Focus	+	-
Automatic recording	-	+
Time required from recording until image available	+	-
Image distortion (combination of images)	+	-
Suitability for monochrome weather maps	+	-
Mechanical extent for manufacture	-	+

Since most points will be evaluated differently, the author considers that both methods possess their distinct advantages.

The electronic circuitry for the FAX-recording is accommodated on four PC-boards in the author's prototype. The present system resulted because the electronic circuit for the mechanical image recording was firstly constructed, and the electronics for the TV-system came later. These modules are to be rearranged for publication in VHF COMMUNICATIONS. The PC-boards now accommodate the following circuits:

1. Frequency processing for the various standard speeds required for the drum motor of the FAX-machine;
2. Output stage for driving the motor
3. Signal processing for modulation of the pin current, or cathode beam;
4. X and Y-deflection, blanking of Z, camera control with counter.

In addition to this, smaller PC-boards are provided for the high-voltage supply, and for the X- and Y-output stages.

After describing the overall system, we can now commence with the detailed descriptions.

2. PARABOLIC ANTENNA WITH TUBULAR RADIATOR

Since the parabolic dish was to be home-made, all parameters could be selected as required. For this reason, the tubular radiator was firstly designed, and a matching parabolic dish was then selected.

2.1. Tubular Radiator for 1693 MHz

The dimensions of a tubular radiator for 2304 MHz described by DJ 1 SL in (3), were recalculated linearly for 1693 MHz. At the selected tube diameter of 120 mm, the resulting dimensions are given in Figure 5. If a brass tube of 120 mm inner diameter is not available, it can be made using 1 mm thick brass plate as in the case of the author. The seam and the base plate were hard-soldered.

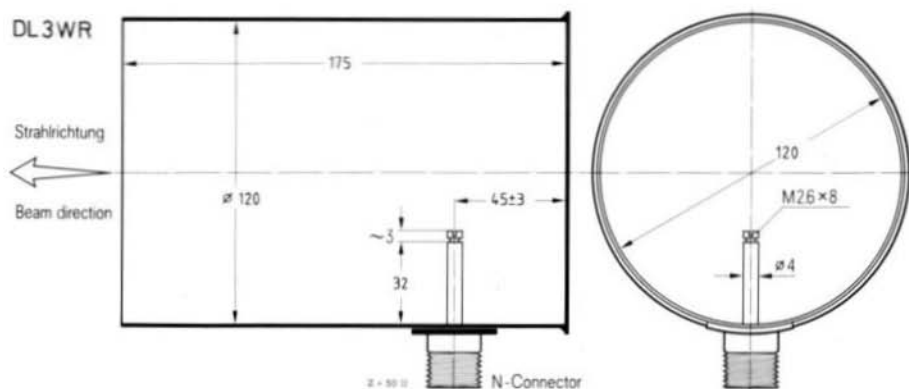


Fig. 5: Tubular radiator for METEOSAT reception for parabolics having f/D of 0.4

The radiator element comprises an N-connector socket and a brass rod of 4 mm diameter which is soft-soldered to the inner conductor. A brass screw of M 2.6 x 8 mm long is provided at the free end of this radiator for exact frequency alignment. The tubular radiator exhibits a 3 dB beamwidth of approximately 80°, and the 10 dB beamwidth is approximately 130°. Based on this, the author designed a parabolic dish with the aid of a colleague.

2.2. Parabolic Dish

As was given in (3), it will be seen that a parabolic dish with a focal angle f/D of approximately 0.4 is suitable for the 10 dB beamwidth of the tubular radiator of approximately 130°. A diameter of 120 cm was selected together with a focal depth of $f = 50$ cm ($f/D = 0.42$). **Figure 6** shows this combination schematically. At this relatively long focus, the curvature is still so low that the deviations from the ideal parabolic that result using the manufacturing system (manufacturing the dish from individual segments) remain sufficiently low and have little effect.

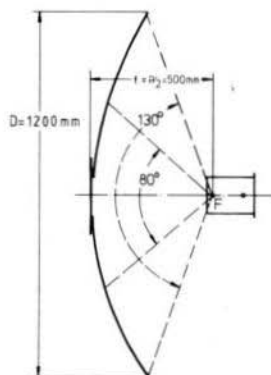


Fig. 6:
The parabolic dish
and radiator together
with the radiator
beam widths

As was mentioned in the introduction, the idea was to construct a parabolic dish from 12 individual segments that could also be drilled before bending. The parabolic shape results after the individual parts are screwed (or rivetted) together. This results in low material costs (less than 2 m² of 1 mm thick aluminium plate), very low tooling costs (1 drilling template) and not to forget the advantages when shipping the parabolic reflector before assembly.

An individual segment with all dimensions is given in **Figure 7**. The lengths given on the left hand side, are based on calculations made from the center point O of the parabolic dish; on the right-hand side, the workshop values are given which are based on the edge that has been cut from the triangular plate. A relatively simple method of manufacturing these pieces is now to be described:

The technical staff of VHF COMMUNICATIONS obtained a strip of 678 mm in width from a 2.5 m long aluminium plate, which was then cut, according to the small diagram, into triangles having the dimensions given in Figure 7. A total of 13 pieces are obtained. The narrow points of the triangle are cut off at the given position so that a length of 550 mm remains. The points of the 12 parabolic segments are now replaced by either a 12-cornered or round plate of approximately 180 mm diameter which is mounted to each segment after assembly with the aid of a screw (or rivet).

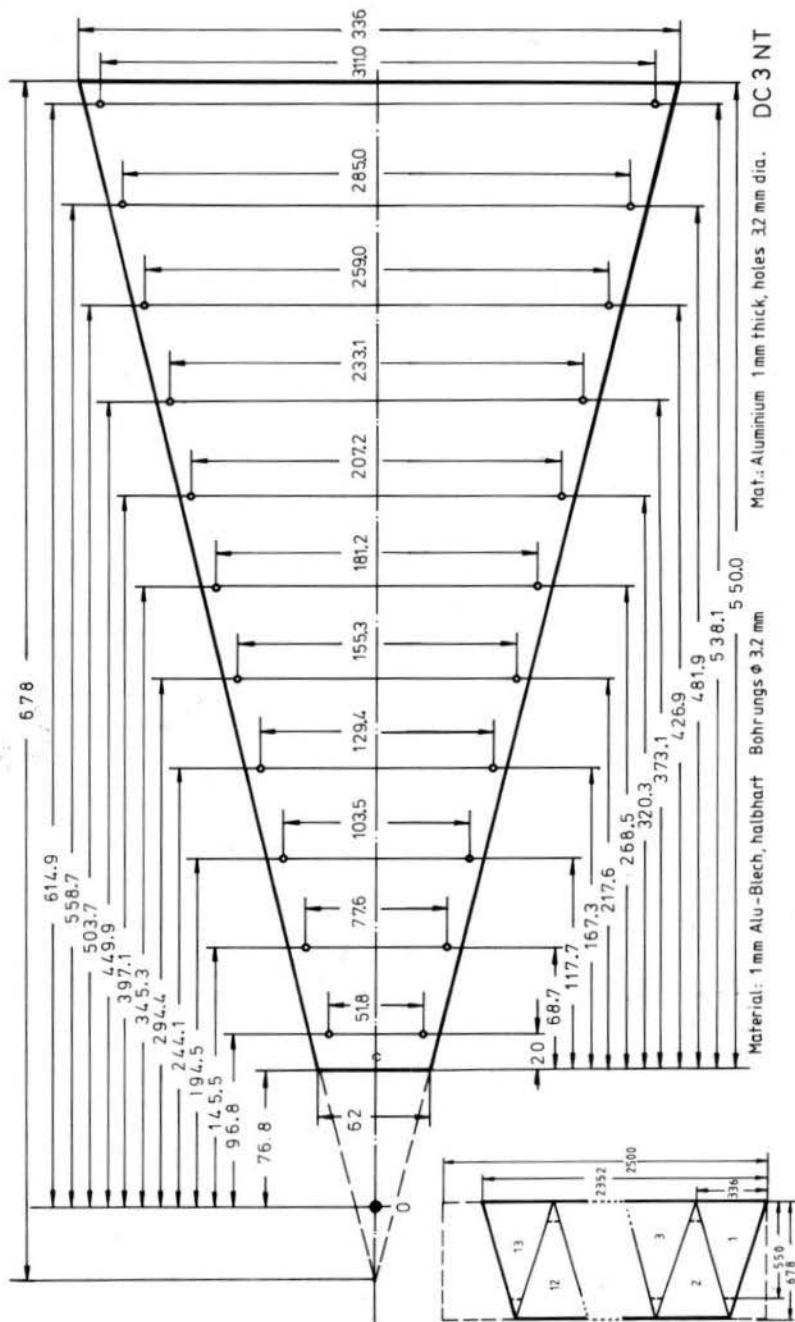


Fig. 7: Dimensions for the 12 segments of the parabolic dish

The mounting of the tubular radiator behind the focal point of the dish (adjustable) with the aid of a ring and tripod (aluminium tube of 10-15 mm diameter), as well as the mounting of the antenna is not to be described in detail here. An idea can be taken from the photograph given in **Figure 8** which shows the prototype antenna at the author's location.

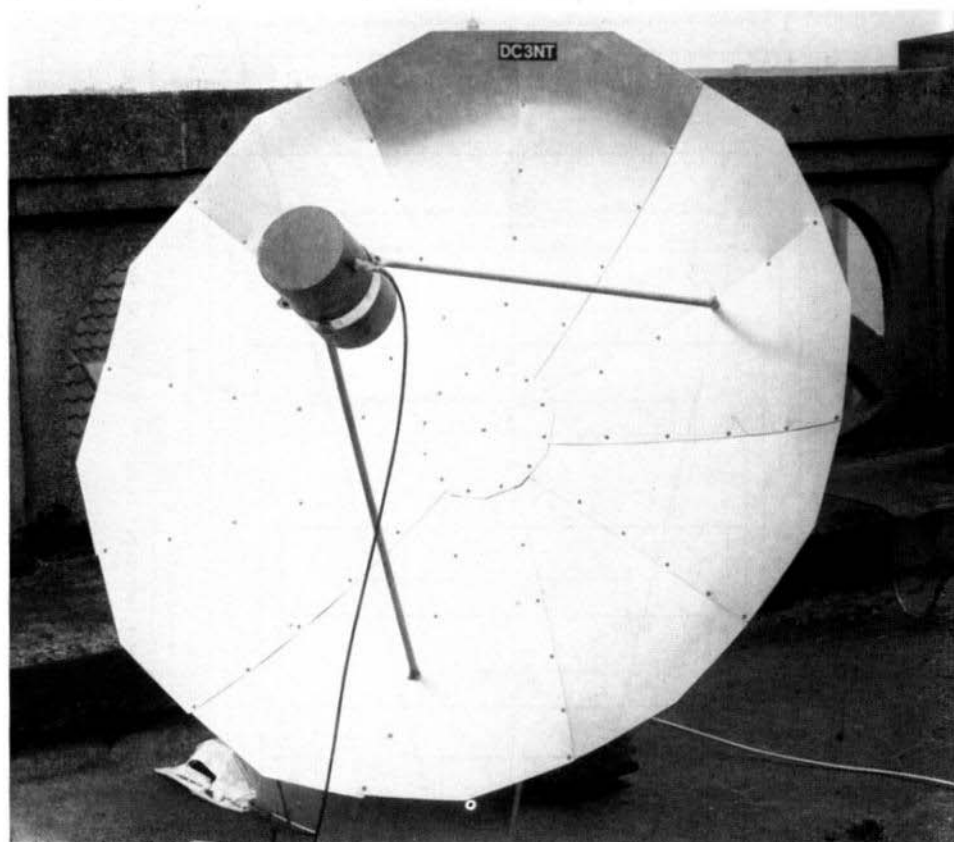


Fig. 8: Photograph of the author's prototype antenna

2.3. Appendix: Calculation of the Parabolic Dish

The calculation of the 12 parabolic segments is based on **Figure 9** which shows a segment without the overlapping required for mounting the segments together.

Where:

- l_{max} = Maximum length (determined by the outer diameter of the dish)
- l_{min} = Cut length (inner diameter of the dish, depending on manufacture)
- b = $1/12$ of the circumference at point $P = f(x)$
- a = Chord associated to b
- c = Vertical associated to a
- α = Angle associated to b

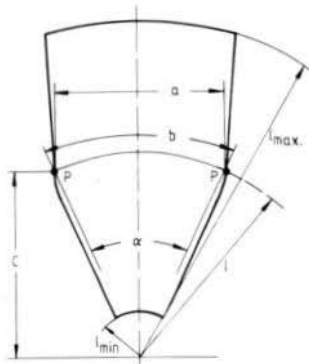
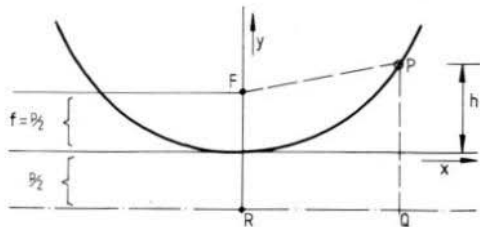


Fig. 10:
The parabolic
characteristic

Fig. 9:
One segment of the dish
(schematically) with the
design magnitudes



The definitions of the parabolic characteristics are now required, and these are given in **Figure 10**;

The following is valid:

Path PF = Path PQ

Path OF = Path OR = $p/2 = f = \text{focus}$

$l = \text{Arc OP}$

$P = x^2 - 2py = 0$

The following equations are derived from this:

$$x^2 - 2py = 0$$

$$y = \frac{x^2}{2p}$$

(1)

$$l = \text{Arc OP} = \sqrt{h \left(h + \frac{p}{2} \right)} + \frac{p}{2} \text{ arc sinh } \sqrt{\frac{h}{p/2}}$$

with $h = y$:

$$l = \sqrt{\frac{x^2}{2p} \left(\frac{x^2}{2p} + \frac{p}{2} \right)} + \frac{p}{2} \text{ arc sinh } \sqrt{\frac{x^2}{2p \cdot x \cdot p/2}}$$

$$l = \frac{x}{2p} \sqrt{x^2 + p^2} + \frac{p}{2} \text{ arc sinh } \frac{x}{p}$$

(2)

$$b = 2x \frac{\pi}{2} \quad (I)$$

$$b = 2l \frac{\pi \cdot x \cdot \alpha}{360^\circ} \quad (II)$$

This results in the following:

$$\alpha = 30^\circ \frac{x}{l} \quad (3)$$

$$a = 2l \sin \frac{\alpha}{2} = 2l \sin \left(15^\circ \frac{x}{l} \right) \quad (4)$$

$$c = \cos \frac{\alpha}{2} = l \cos \left(15^\circ \frac{x}{l} \right) \quad (5)$$

With the aid of the given equations, segments of parabolic dishes were calculated with various focal depths ($f = 40$ cm, 45 cm, 50 cm, 55 cm and 60 cm) and up to a diameter of 2 m. A Hewlett-Packard computer was available for this. For construction, a dish of $f = 500$ mm and $D = 1.2$ m was selected. The original computer print-out for $p = 1000$ mm ($\triangleq f = 500$ mm) is now to be given.

```

100 DEG
110 FIXED 2
120 FOR P=800 TO 1200 STEP 100
130 PRINT PAGE
140 PRINT "P=";P;L:IN(5)
150 PRINT CHR(132);" X Y L A C"
ALPHA="";CHR(128);L:IN(2)
160 FOR X=50 TO 1200 STEP 50
170 L=X+SQR(X*(X+P))/(2+P)+P*LOG(X/P+SQR(X*(X+P)/(2+P)))/2
180 Alpha=15*X/L
190 A=2*L*SIN(Alpha)
200 C=L*COS(Alpha)
210 V=X*(X/(2+P))
220 PRINT USING 230;X;V;L;A;C;Alpha
230 IMAGE (DDDDDD,DD,2X)
240 NEXT X
250 PAUSE
260 NEXT P
270 END

```

P= 1000.00

X	V	L	A	C	ALPHA
50.00	1.25	50.02	25.88	46.32	14.99
100.00	5.00	100.17	51.77	96.76	14.98
150.00	11.25	150.56	77.65	145.47	14.94
200.00	20.00	201.33	103.54	194.55	14.90
250.00	31.25	252.58	129.44	244.15	14.85
300.00	45.00	304.44	155.34	294.37	14.78
350.00	61.25	357.02	181.25	345.33	14.71
400.00	80.00	410.42	207.17	397.14	14.62
450.00	101.25	464.76	233.10	449.90	14.52
500.00	125.00	520.11	259.04	503.73	14.42
550.00	151.25	576.59	285.00	558.70	14.31
600.00	180.00	634.27	310.96	614.92	14.19
650.00	211.25	693.24	336.93	672.45	14.06
700.00	245.00	753.56	362.92	731.39	13.93
750.00	281.25	815.32	388.91	791.79	13.80
800.00	320.00	878.50	414.92	853.74	13.66
850.00	361.25	943.41	440.94	917.28	13.51
900.00	405.00	1009.85	466.97	982.48	13.37
950.00	451.25	1077.96	493.02	1049.39	13.22
1000.00	500.00	1147.79	519.07	1118.07	13.07
1050.00	551.25	1219.40	545.13	1188.54	12.92
1100.00	605.00	1292.81	571.21	1260.87	12.76
1150.00	661.25	1368.07	597.29	1335.07	12.61
1200.00	720.00	1445.22	623.38	1411.21	12.45

REFERENCES TO PART 1

- (1) T. Bittan: Reception of the METEOSAT Weather Satellite VHF COMMUNICATIONS 10, Edition 3/1978, pages 169 - 172
- (2) R. Lentz: More Details on Reception of the European Weather Satellite «METEOSAT» VHF COMMUNICATIONS 10, Edition 4/1978, pages 230 - 240
- (3) H. J. Griem: A Tubular Radiator for Parabolic Antennas on the 13 cm Band VHF COMMUNICATIONS 8, Edition 4/1976, pages 207 - 214

A FREQUENCY DOUBLER FOR THE 13 CM BAND WITH 6 W OUTPUT POWER

by O. Frosinn, DF 7 QF

The doubler to be described in the following article is equipped with a varactor diode type BXY 27 (Philips) and is suitable for frequency doubling from the order of 1152 MHz to approximately 2304 MHz. Its maximum output power amounts to 6 W. It can be constructed, without extensive lathing and milled parts, easily from epoxy PC-board material, brass tube or bars (6 and 7 mm in diameter), several M 3 and M 6 screws and nuts, as well as BNC connectors type UG-1094. The construction and the most important dimensions are given in Fig. 1.

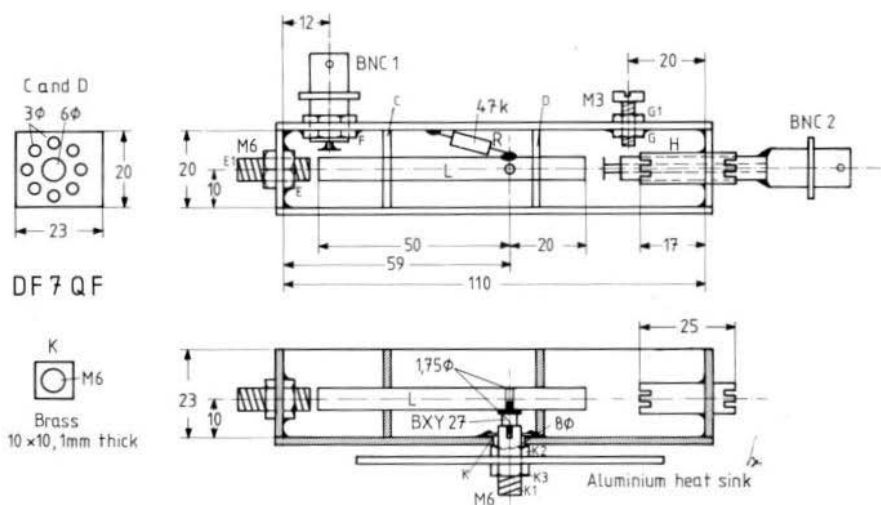


Fig. 1: Power frequency doubler 1200/2400 MHz

1. CONSTRUCTION

Firstly, the epoxy PC-board material is sawn to the right sizes and provided with the required holes. The dimensions should be adhered to as closely as possible. After this, nuts E, F, and G are soldered into place, as well as the slotted brass tube H. Finally, the various parts of the case are soldered together cleanly. If corresponding taps are available, the holes for E 1, G 1, and BNC 1 can be in the form of tapered holes.

The protruding piece of PTFE dielectric is removed from BNC 1, the inner conductor cut down to a 3 mm in length, and a circular disk of 6 mm dia. of brass or copper plate soldered into position here. An approximately 40 mm long brass tube, or copper wire of 2 mm dia., is soldered to the inner conductor of BNC 2. Finally, a 6 mm brass tube of 38 mm in length is soldered to the edge of the connector. Attention should be paid during this that the tubes are coaxial and centrally mounted to the connector. This is achieved at the open-end by insert-

ing the PTFE piece cut from BNC 1. The original 40 mm long inner conductor is now shortened so that it protrudes 4 mm from the 6 mm tube, and provided with a disk of 5 mm in diameter. It is now possible for this coupling probe to be placed in the slotted end of the 7 mm tube that has been pressed together slightly.

Spacers C and D are made from epoxy PC-board material from which the copper coating has been removed. They should be of such size that they are jammed lightly into the chamber. The mounting and heat dissipation screw K 1 (M 6, brass) is provided with a 3 mm deep, 1.75 mm dia. hole. This is made most favorably, of course, in a lathe. However, if the screw is marked exactly with the center point and a new 1.75 mm drill is used, it should be possible for it to be made on a drill stand. The hole should not be noticeably outside of the center, since the diode could easily be damaged on tightening screw K 1. The exact diameter of the hole ensures a good fit to the diode, and is thus necessary for efficient heat dissipation.

The hole in the inner conductor L can have a somewhat greater diameter than 1.75 mm, since the anode flange of the BXY 27 has a diameter of 3 mm. It is thus possible for it to be increased to 2 or even 2.25 mm. Part K is now screwed on to screw K 1. Part K 1, in turn, protrudes through the 8 mm hole in the case and is slightly countered using nut K 2. Spacers C and D are pushed over the inner conductor L and placed into the case. By alternately shifting L and K 1, the holes for the diode are centered: firstly optically, after which a 1.75 mm drill is placed through L into K 1. Plate K is now soldered to the base of the case at any position that can be reached, parts C, D and L are then removed and K soldered all around. Attention should be paid during this that K is not shifted. Finally, C, D, and L are reinstalled, the holes centered again, and parts C, D, and L are glued into position with a fast drying glue, if required. The diode should be inserted to see if it fits. If it fits, parts C, D, and L can be finally glued into place using a dual-component glue.

After hardening, resistor R (47 k Ω /0.5 W) is soldered into place after firstly removing the diode. A miniature trimmer potentiometer of 50 k Ω is also very suitable after the rotating part has been removed. The diode hole in K 1 should now be filled with very little heat-conductive paste, K 1 and the diode are then mounted, and a heat sink screwed onto this using a second nut K 2. The extensive description of the diode mounting seems very complicated, but it has the advantage of good heat dissipation and allows a simple exchange of the diode. If K 1 is made from copper, the heat dissipation will be even better.

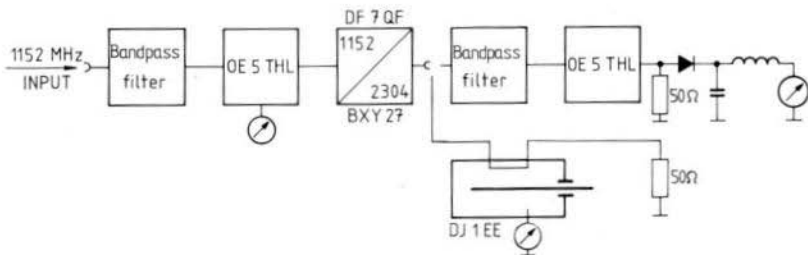


Fig. 2: Alignment setup

2. ALIGNMENT

For the alignment process, BNC 1 is connected via a VSWR-meter, e.g. like that described in (1), to a 1152 MHz exciter with an output power at first in the order of 100 mW. The output is connected via a bandpass filter for 2304 MHz (2) to a 50 Ω detector, or via a coaxial wave-meter (3) to a 50 Ω terminating resistor. **Figure 2** shows this schematically.

The alignment for minimum VSWR at the input and maximum output power at the output is achieved by shifting BNC 2, rotating BNC 1, and aligning M 3. The output probe is finally approximately 3 to 4 mm from the inner conductor L. The drive power is now increased in steps and the alignment carefully corrected. Finally, the drive power at 1152 MHz will be a maximum of 12 W, which then results in approximately 6 W output at 2304 MHz. The efficiency is dependent on the drive power, and achieves a maximum in the case of the author's prototype of approximately 65 % at a drive power of approximately 6 W.

Experiments were also made using diode type BXY 28, and the described construction is also suitable for the use with this diode; however, the drive power should not be more than a maximum of 5 W. A maximum efficiency of 75 % was measured. **Figure 3** finally shows in the form of a block diagram how sufficient power can be obtained at 1152 MHz using modules that had already been described in VHF COMMUNICATIONS. This exciter can be keyed or frequency-modulated. The diagram can be read that each of the vertical columns can be used to form a block as required. The upper three are semiconductor versions, the lower are versions equipped with tubes. When a subsequent varactor mixer is used, the high power can also be converted into a SSB signal (4).

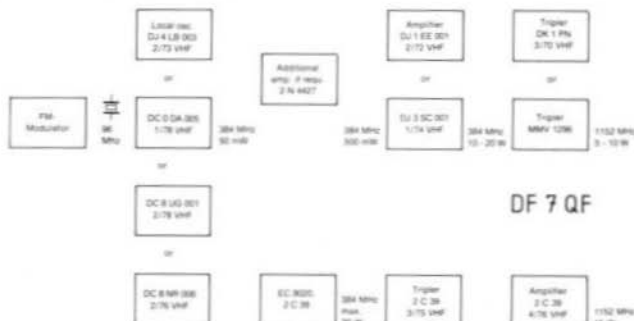


Fig. 3: Variations to form an exciter

3. REFERENCES

- (1) H. Tiefenthaler and B. Rößle: A Precision Reflectometer for 0 to 2300 MHz
VHF COMMUNICATIONS 6, Edition 1/1974, pages 2 - 17
- (2) D. Vollhardt: Narrow-band Filters for the 23 cm, 13 cm, and 9 cm Bands
VHF COMMUNICATIONS 10, Edition 1/1978, pages 2 - 11
- (3) K. Hupfer: An SHF Wavemeter
VHF COMMUNICATIONS 7, Edition 2/1975, pages 90 - 92
- (4) H. Fleckner: An SHF Transmit Converter with a Varactor Diode
with High Efficiency and Low Intermodulation
VHF COMMUNICATIONS 10, Edition 1/1978, pages 12 - 37

SSB-TRANSMIT MIXERS FOR THE SHF BANDS

Part 2: The 9 cm Band

by R. Heidemann, DC 3 QS

Since the SSB-transmit mixer to be described for the 9 cm band operates according to the same theory as was described for the 13 cm version given in part 1, the same principles are valid and are not to be repeated here. A signal frequency of 144 MHz has been selected since it offers the best compromise between spurious rejection and ease of operation (portable operation is possible). This means that the required oscillator frequency is 3312 MHz ($3312 + 144 = 3456$ MHz). The necessary UHF and SHF varactor multipliers are to be described in this article. It is also possible when using these varactor circuits to multiply the output frequency from a 70 cm transmitter in the A 1 and F 3 modes to output frequencies in the 9 cm band.

1. A LINEAR TRANSMIT MIXER FOR THE 9 cm BAND

As was mentioned in Part 1, the 9 cm power mixer is also to be constructed in the form of a printed hybrid ring on a double-coated PTFE-glassfibre board. **Figure 1** shows the circuit of the mixer together with several construction details.

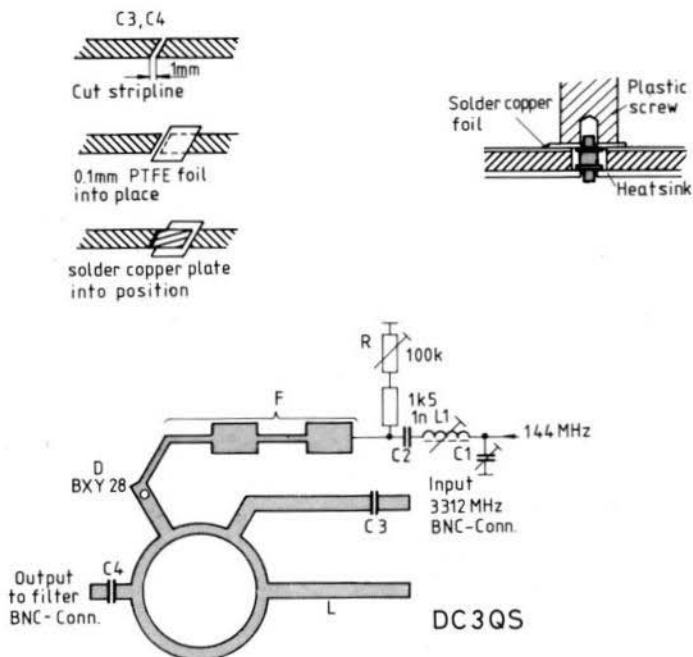


Fig. 1: An SSB-mixer for 9 cm in microstrip technology with construction details

The 2 m input signal is matched to the largely capacitive input of the mixer with the aid of the network comprising L 1 and C 1. The 144 MHz signal is fed to the phase modulator via the low-pass filter comprising four $\lambda/4$ impedance jumps. Extensive experiments have shown that the diode type BXY 28 is most suitable for this application, since it is very favourable with respect to efficiency and price. The open 50Ω microstripline L serves as standard impedance to convert the phase modulation into the required amplitude modulation. For price reasons, no special trimmer is used at this position, but the fine adjustment of the phase angle φ_0 is made with the aid of trimmer R. This is possible because a portion of the 3312 MHz signal is rectified in the varactor. The DC-current produces a DC-voltage drop across R, which is used as bias voltage for the junction capacitance of the varactor D, and is thus able to influence the phase angle φ_0 .

Capacitances C 2, C 3 and C 4 (see Fig. 1) are used as DC isolators; C 3 and C 4 also ensure that no 2 m energy can enter the connected local oscillator chain, or be virtually short circuited by the a 9 cm interdigital filter at the output.

Figure 2 shows a photograph of the author's prototype. The components are:

- L 1: 2 turns of 1 mm diameter silver-plated copper wire on a 5 mm coilformer with core
- C 1: Plastic foil trimmer 30 pF (red)
- C 2: 1 nF ceramic disc capacitor without connection wires
- C 3, C 4: Constructed from PTFE-foil and copper foil according to Fig. 1

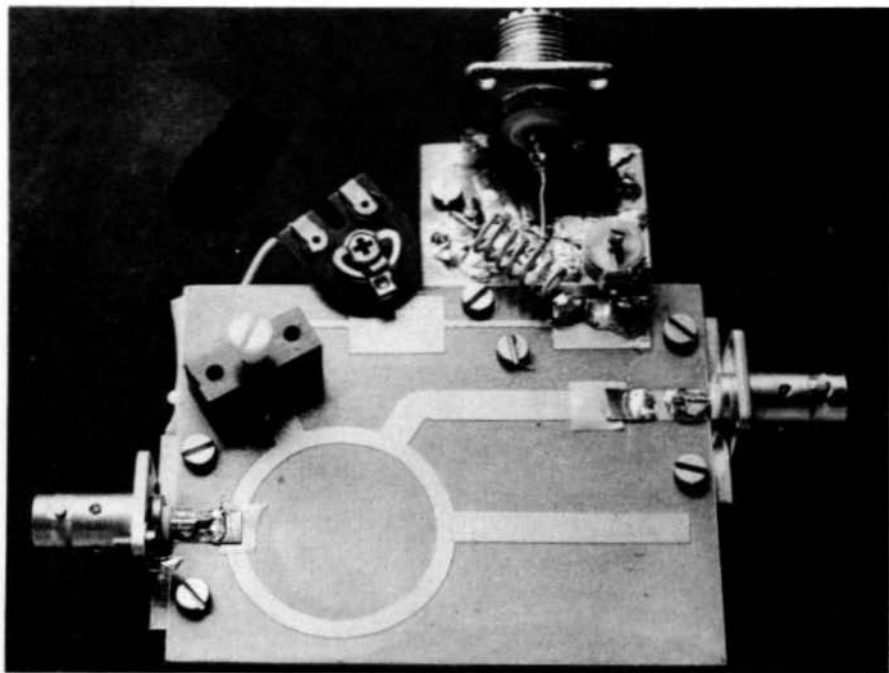


Fig. 2: Photograph of the author's prototype

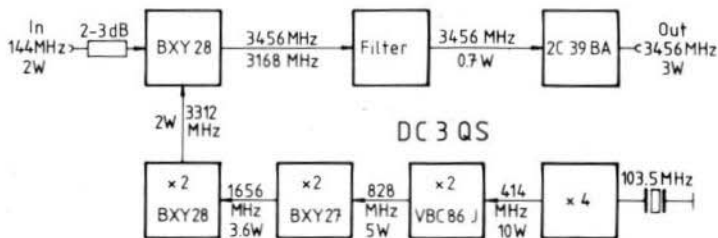


Fig. 3: Block diagram of the 9 cm SSB mixer

2. LOCAL OSCILLATOR FOR 3312 (3456) MHz

Several efficient power amplifiers for the 400 MHz range have been described in this magazine. Required for our application is one for 414 or 432 MHz with an output power of 10 W. The description of the author's local oscillator for the 9 cm transmitter (**Figure 3**) is therefore to begin with the three doubler stages. This multiplier chain represents the optimum means of obtaining the required output signal for SSB-applications, especially with respect to its cost, efficiency, ease of construction, and spectral purity of the oscillator signal. As a conclusion, a very simple multiplier (by 4) is to be described for A 1 and F 3 transmitters: $828 \times 4 = 3312$ or $864 \times 4 = 3456$ MHz.

Figures 4 a and 4 b show the construction of a frequency doubler from 414 or 432 MHz to 828 or 864 MHz. The circuit is built up on the copper side of a suitable piece of PC-board (epoxy) material and mounted on a heatsink. PC-board material is also used to form the side panels and cover to construct a screened box. **Figure 4 c** shows a photograph of the author's prototype. The components required are:

Tr 1, Tr 3 - Tr 6: 3.5 pF ceramic miniature spindle trimmers

Tr 2: 5 pF plastic foil trimmer (grey) 7 mm diameter

L 1, L 2: 3 turns of 1 mm dia. silver-plated copper wire, self-supporting, inner dia. 7 mm

L 3, L 4: Thin copper strip 5 mm wide, 7 mm high, and length:
L 3: 26 mm; L 4: 22 mm

Diode and BNC conn. see text.

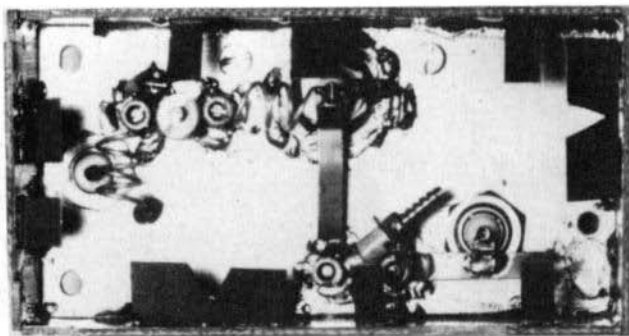


Fig. 4c

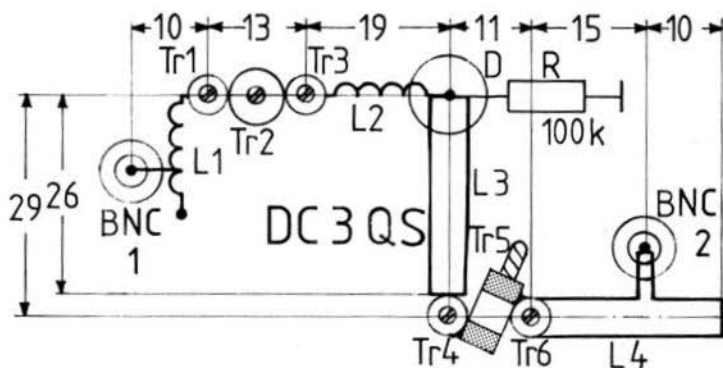
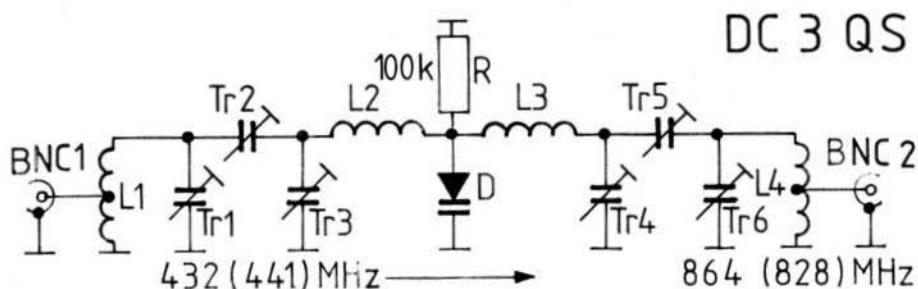


Fig. 4: The 400/800 MHz doubler circuit with dimensions and construction details

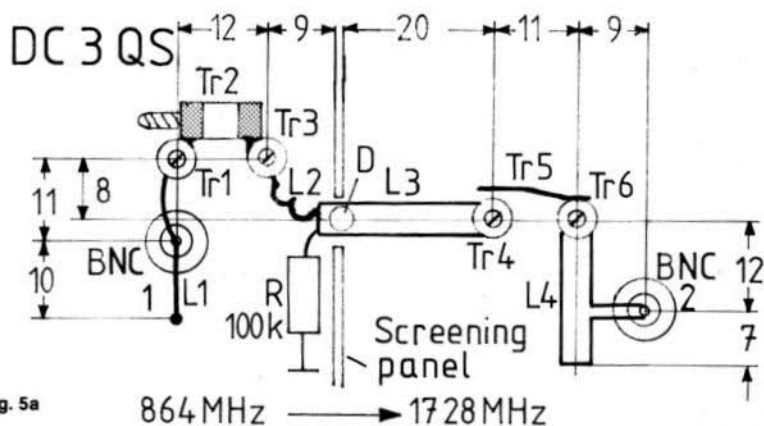


Fig. 5a

The frequency doubler from 828 or 864 MHz to 1656 or 1728 MHz is shown in **Figures 5 a to 5 d**. The construction and alignment of this module are also uncritical. The following diodes are suitable for this multiplier and also the previous 400 to 800 MHz doubler: BAY 66, VBC 86 J, VEC 87 M, BAX 11 and possibly BXY 27. The other components required for the frequency doubler shown in Fig. 5 are:

- Tr 1 - Tr 4, Tr 6: 3.5 pF ceramic miniature spindle trimmers
 Tr 5: Copper plate of 4 mm wide and 14 mm long
 L 1: 25 mm long piece of 1 mm dia. silver-plated copper wire
 L 2: 1 turn of 1 mm dia. silver-plated copper wire, self-supporting, inner dia. 7 mm
 L 3, L 4: Thin copper plate of 4 mm wide and 4 mm high, length:
 L 3: 20 mm; L 4: 17 mm

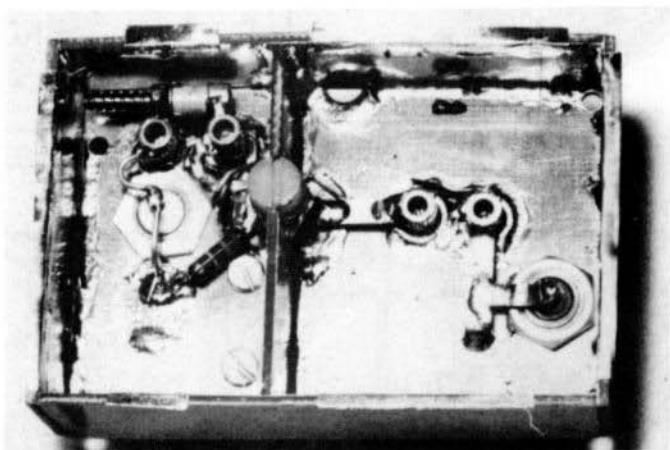
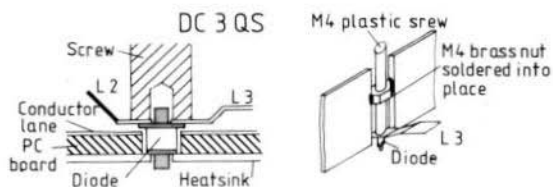


Fig. 5: Dimensions, construction details and a photograph of the author's 800/1600 MHz doubler

The construction of the frequency doubler from 1656 or 1728 MHz to 3312 or 3456 MHz is more complicated since very small coaxial circuits are to be soldered together from PC-board material. The complicated construction shown in **Figure 6** was selected since it allows external adjustment of all seven (!) alignment points, which means that it is not necessary to keep opening and resealing the unit. Due to the versatility of the alignment of the output circuit (2 for coupling, 1 for capacitive tuning), it is possible for the 3312 MHz oscillator chain to be matched favourably to the SSB-mixer, which is often a problem with other types of multipliers. In our case, the output circuit is directly connected to the mixer using a BNC coupler (2 BNC conn. UG-491/U) without interconnection cable.

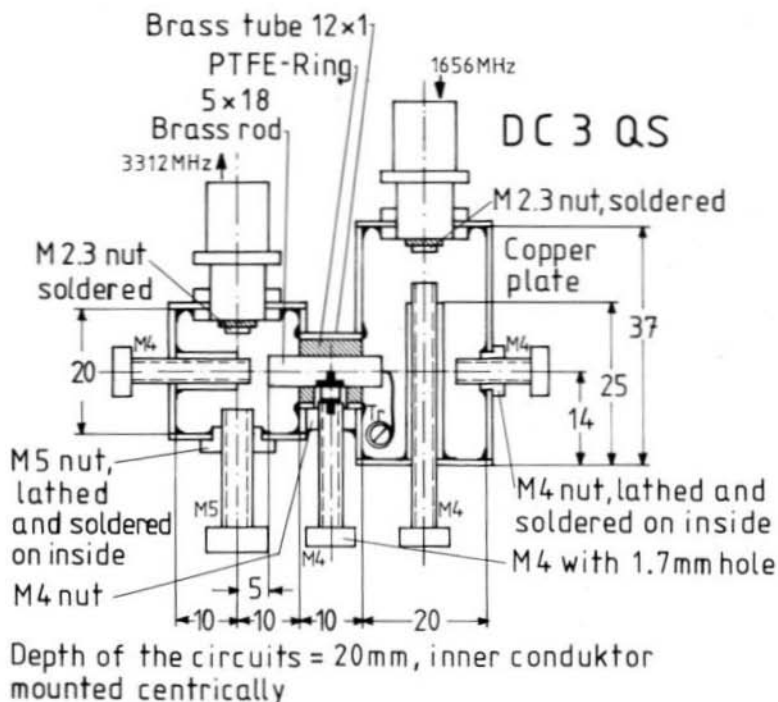


Fig. 6: The 1600/3200 MHz doubler

The varactor diode type BXY 28 has been found to be extremely suitable in practice. In order to avoid the usual dropper resistor which is unfavourable in the coaxial circuits, the ceramic case of the diode is coated with graphite from a pencil so that the junction resistance in the reverse direction drops to approximately 20 k Ω . This multiplier can be modified to form a tripler or quadrupler by lengthening the input circuit.

A quadrupler from 828 or 864 MHz to 3312 or 3456 MHz in the form of an interdigital filter is shown in **Figure 7**. This multiplier can be easily constructed from PC-board material, represents no problems with respect to the circuitry, and can be used as tripler. The open $\lambda/4$ line L 3 is designed for 3312/3456 MHz and allows the current flow through the diode at the required output frequency. It is possible in the same manner to provide idler circuits at this position for the second and third harmonics of the input frequency. The tapping point on circuit L 4 has been optimized for diode types BXY 38 and BXY 28; in the case of other diodes it may be necessary to vary this. An efficiency of 15 % to 20 % will be exhibited.

The components for this quadrupler are:

- Tr 1: Plastic foil trimmer 22 pF (green)
- Tr 2, Tr 3: Plastic foil trimmer 12 pF (yellow)
- R: Approx. 1.8 k Ω
- L 1, L 2: 1 mm diameter silver-plated copper wire
L 1: Length 27 mm, Height 4 mm; L 2: Length 22 mm, Height 4 mm

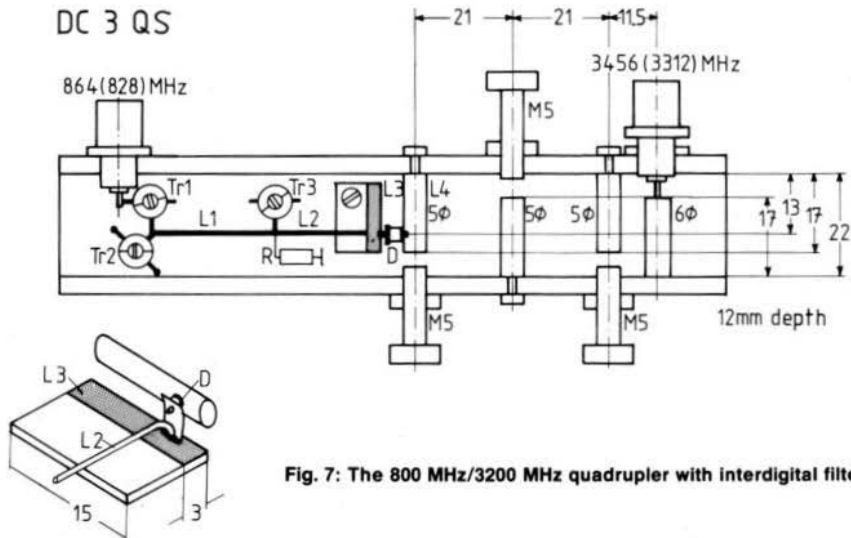


Fig. 7: The 800 MHz/3200 MHz quadrupler with interdigital filter

3. ALIGNMENT AND SPECIFICATIONS

The alignment of varactor multipliers has been described many times and need not be repeated here. It is only important to know that the tendency to parasitic oscillation is lower the lower the DC resistance of R. Varactor multipliers that are connected in series are aligned one after another into a terminating resistor, this is achieved at first by connecting 3 dB pads between each multiplier. The alignment of the previous multiplier should then remain unaltered.

The author has used a chain of three doublers under various operating conditions (different input powers at 414 MHz, temperature variations during mobile operation etc.), which worked reliably without intermediate attenuator pads. For alignment and operation of the mixer, it should be connected as shown in Figure 3 to the local oscillator chain, a 2 m transmitter with 1.5 - 2 W output (insert 2 to 3 dB attenuation for isolation), and terminated through a pre-aligned 3456 MHz filter by a power meter. With the oscillator switched on, the 144 MHz input circuit L 1 + C 1 is aligned for minimum VSWR. The varactor bias voltage is adjusted at resistor R, and the 3312 MHz circuit of the last doubler aligned for maximum output power in the 9 cm band. Finally it is possible to optimize the alignment of the 9 cm filter carefully. This alignment should, if possible, be made with the aid of a spectrum analyzer to ensure that it is not aligned to the maximum sum voltage of these 3 frequencies (3456, 3312, and 3128 MHz).

The described modules should provide the following specifications when interconnected as shown in Figure 3:

Input power at 414 MHz:	10 W
Power at 828 MHz:	51 W
Power at 1656 MHz:	3.6 W
LO power at 3312 MHz:	2.0 W
SSB output power at 3456 MHz:	0.7 W

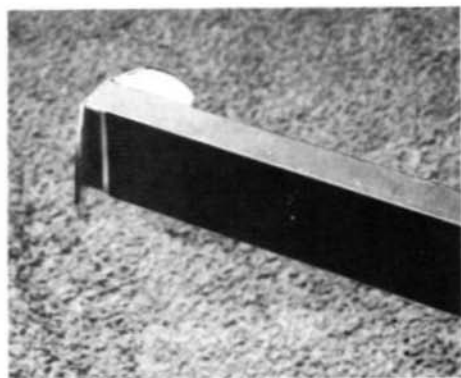
A SIMPLE RADIATOR FOR 3 cm PARABOLIC DISHES

by R. Heidemann, DC 3 QS

Parabolic dishes are becoming more and more popular on the microwave amateur bands, mainly due to the fact that they provide a favourable relationship between gain and mechanical construction work involved.

In order to guarantee maximum gain, it is necessary to ensure that the parabolic dish is fully illuminated. Horn or tubular radiators (1) are very suitable for home construction, since their radiating characteristics (beamwidths) and thus their mechanical dimensions can be easily calculated to suit an available dish. One distinct disadvantage of using a horn radiator on the 3 cm band is the difficulty of mounting the waveguide feed.

An X-band radiator that is popular in radar applications is to be described that represents a suitable alternative to horn, tubular, and dipole radiators. The feed to be described is suitable for dishes having a focal angle f/D of 0.58. The only materials required for construction are a piece of R 100 (WG 16) waveguide, and a 1 mm brass plate of 26 mm by 62 mm.

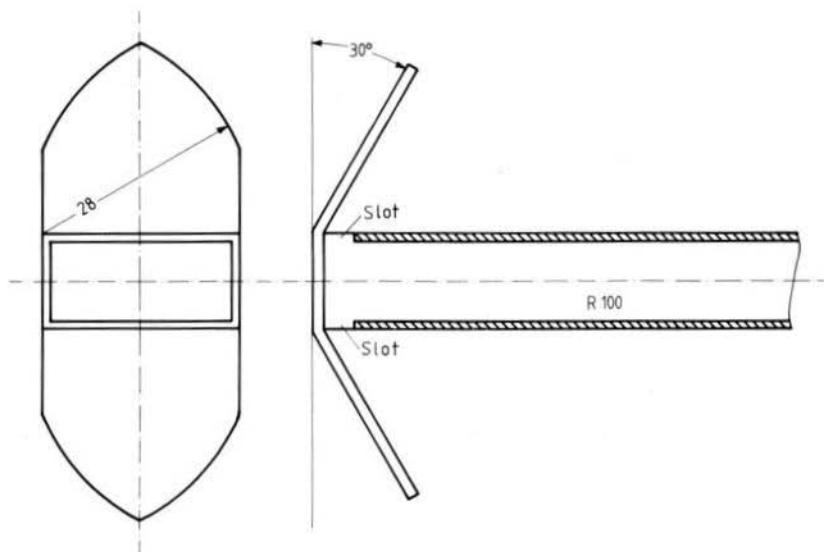
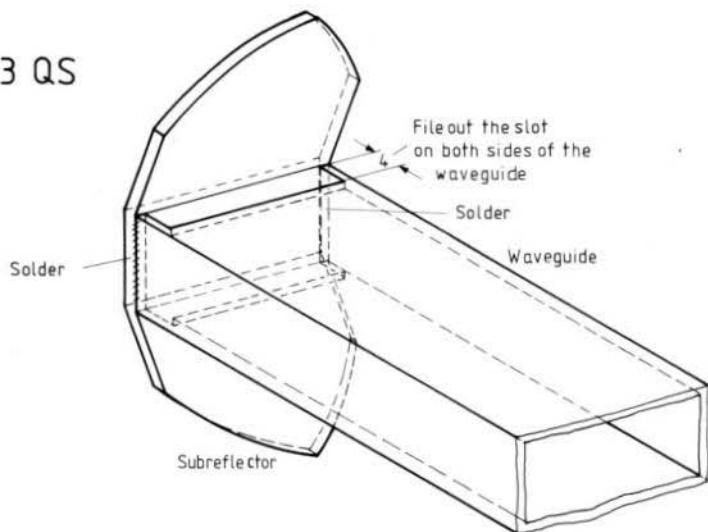


Figures 1 and 2: A 38 cm diameter antenna for 10 GHz

Figure 1 shows the feed mounted in a 15" parabolic dish having a f/D of 0.58, which is suitable for use with it. The feed itself can be seen in more detail in **Figure 2**. Construction information is given in **Figures 3 and 4**.

The radiator is constructed by filing down the wide sides of the waveguide by 4 mm. The brass plate is then prepared as shown in **Figure 4** and soldered to the remaining narrow sides of the waveguide, after which the plate should be bent towards the dish to form the required angle of 30°.

DC 3 QS



Construction of the subreflector
M 1:1

Figure 3: The contours of the sub-reflector can be traced onto the metal plate

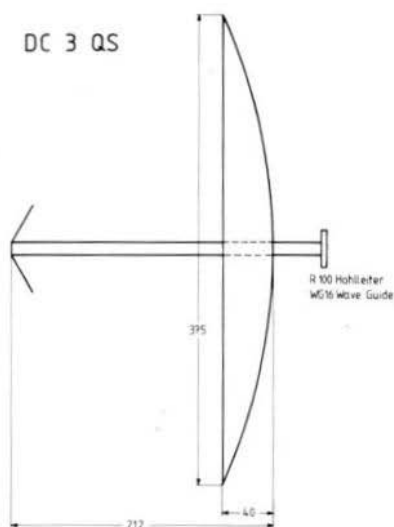


Fig. 4:
Dimensions of the antenna
shown in Fig. 1

The mounting of the feed will depend on the dish used, and no details can be given here. However, it is advisable for the feed to be made adjustable in the axial direction (spacing to the dish) so that the illumination of the dish can be optimized. Matching can be improved by providing a two-screw tuner. The VSWR will be in the order of 1.2 in the frequency range of interest when aligned for maximum gain.

REFERENCES

- (1) H.J. Griem: A Tubular Radiator for Parabolic Antennas on the 13 cm Band
 VHF COMMUNICATIONS 8, Edition 4/1976, Pages 207-214
- (2) R. Griek and M. Münich: A 3 cm Primary Radiator for Parabolic Antennas
 VHF COMMUNICATIONS 11, Edition 2/1979, Pages 74-75
- (3) A. C. Studd: A Rear Feed for Paraboloidal Reflectors
 The Microwave Journal, February 1966

Back Copies of VHF COMMUNICATIONS

Please remember that we have continued to reprint these editions since each is like a small handbook in itself. Do not forget there are no news columns and other information that becomes out-of-date, and the magazines contain only technical articles, most of which are still state-of-the-art today. All back copies are available back to 1970. We can offer these volumes at the following prices:

Any three volumes	DM 36.00
Any six volumes	DM 65.00
All nine volumes (1970-1978)	DM 95.00

**UKW-TECHNIK / UKW-BERICHTE · Hans DOHLUS oHG · D-8523 BAIERSDORF ·
 Postfach 80 · Jahnstr. 14 · Telefon (09133) 855 + 856 (Anrufbeantworter) · Telex: 629 887**

OPTIMUM SPACINGS OF DIRECTIONAL ANTENNAS

by G. Hoch, DL 6 WU

There have been a number of articles (1-4) that have dealt with the stacking of directional antennas. However, there is still a lot of confusion and misunderstanding among radio amateurs. Very often, a radio amateur will find that the expense and effort involved to obtain the maximum theoretical gain increase of 3 dB on doubling the antenna size has not been achieved in practice. For this reason, it seems advisable to go into the various relationships in more detail.

The basic principles are valid for all types of antenna groups, even if this article is to be based mainly on the Yagi antennas, since this represents the most important application.

1. GAIN OF A DIRECTIONAL ANTENNA

The gain of a directional antenna will, assuming that no losses occur due to side lobes and dissipation, be determined by the beamwidth of the directional characteristic. Kraus (5) used the following equation for this:

$$G_i = \frac{4 \pi}{\Theta_E \times \Theta_H} \quad (1 a)$$

where Θ_E and Θ_H are the angles between the 3 dB points of the E or H-diagram. G_i is the gain over an isotropic radiator. For angles in degrees, and gain in dB over a dipole, the equation will be as follows:

$$G_d = 10 \log \frac{41253}{\Theta_E \times \Theta_H} - 2.14 \quad (1 b)$$

According to this, an increase of gain can only be obtained by decreasing the beamwidth; decreasing the beamwidth by half in one plane will cause a doubling of the power gain (3 dB). If the possibilities of increasing the gain of an individual antenna have been used to the full – for example by lengthening the boom of a Yagi antenna (6) – a further increase of gain can only be obtained by forming groups of antennas. This is to be discussed in this article.

2. THE SUPERPOSITION PRINCIPLE

The radiation characteristic of a group of identical directional antennas results by multiplication of two components:

1. The characteristic of an identical array of (isotropic) elementary radiators
2. The characteristic of one of the directional antennas to be combined (2). Prerequisite is, however, that no interaction takes place.

If the antennas are to be stacked in both planes, it will be necessary to know the individual characteristics of the antenna in both (polarization) planes.

The characteristics of point (isotropic) sources in various arrangements and spacings are to be found in any good antenna handbook. Large arrays can be combined from several sub-groups. However, since mainly groups of two or four antennas are used for amateur radio applications, the following description is to be limited to the relatively clear case of stacking two antennas in the H-plane (two horizontally polarized Yagis stacked one above the other).

2.1. Diagram of two Point-Sources

Two equal-phase point sources will provide the maximum field strength at all points where their waves arrive at identical phase, and a minimum where anti-phase conditions exist, i.e. $(2n - 1) \times 180^\circ$ phase shift. In the case of **Figure 1**, the maximum field strength will be obtained in the symmetrical axis, and the first null is exhibited at the angle φ_1 .

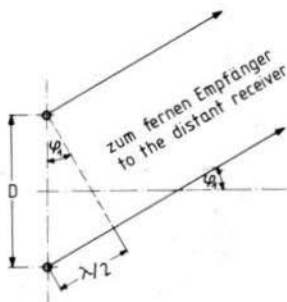
As can be seen in the diagram, the following is valid:

$$\sin \varphi_1 = \frac{\lambda}{2 \times D} \quad (2)$$

The angle for the second null will result when the path difference amounts to $3/2 \lambda$, $5/2 \lambda$, and so on.

The prerequisite for the appearance of a null is a spacing D of at least $\lambda/2$, otherwise, a path difference of $\lambda/2$ will not be possible (smaller spacings are thus unsuitable).

Fig. 1:
Superimposition of the beams of two equal-phase point sources



At $D = \lambda/2$, the null will be at $\pm 180^\circ$, and a polar diagram will have the form of a horizontal Eight. If D is greater than $\lambda/2$, side lobes will appear in the diagram at right angles to the central axis, and will break up into a number of smaller lobes on increasing the spacing D . The first zero-position becomes then nearer and nearer to the central axis.

If D is large with respect to λ , this will result in a large number of narrow lobes. For $D = 10 \lambda$, for instance, the first null will be at $\pm 2.9^\circ$, the second at $\pm 8.6^\circ$, the third at $\pm 14.5^\circ$.

2.2. Diagram of two Stacked Yagis

If the diagram of the point sources is multiplied by the H-diagram of a Yagi antenna, the zero points will be present in all cases. This can be seen easily since the antenna array will not radiate anything in a direction where the individual antenna does not. It will be found that the characteristic of the individual antenna tends to envelope the overall characteristic. The diagrams taken from (1) for two stacked 3-element Yagis show this principle clearly (**Figure 2**). The diagrams show the polar diagrams of the relative field strength in the H-plane in a linear scale. Each diagram is referenced to the maximum value, which means that a direct comparison is not possible.

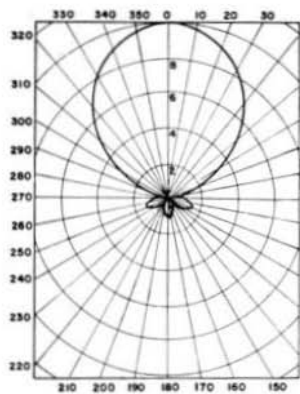


Fig. 2a

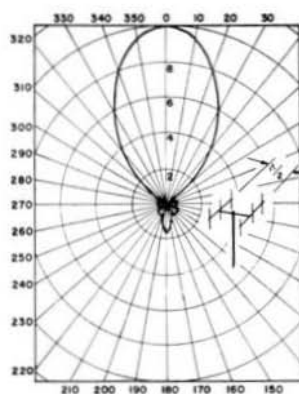


Fig. 2b

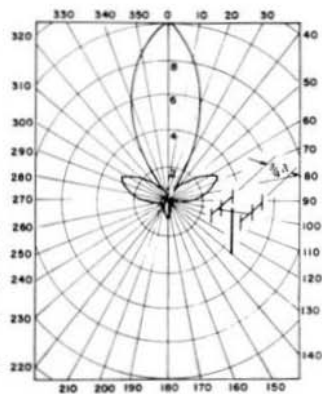


Fig. 2c

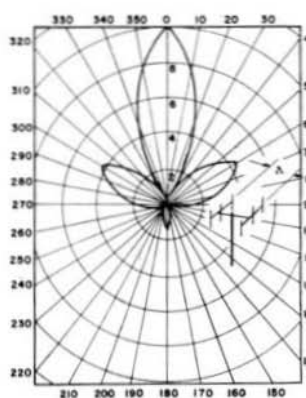


Fig. 2d

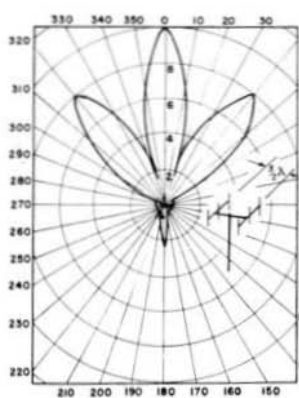


Fig. 2e

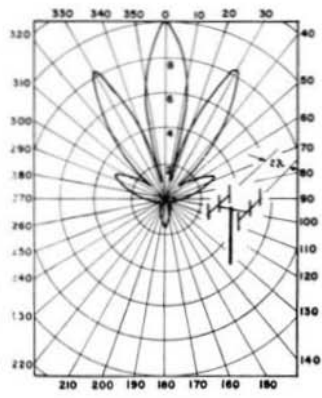


Fig. 2f

Fig. 2: Horizontal diagrams of two vertically polarized, horizontally stacked 3-element Yagis at various stacking distances

3. OPTIMUM SPACING

As is to be expected, large spacings will provide a stacking gain of virtually 3 dB. This is because the field components will subtract over half of the directions in space and add in the other half; this means that the total energy remains equal. The optimum stacking distance is the lowest spacing at which the gain is virtually doubled.

As was seen in the gain equation, it is necessary for the beamwidth of the main beam to be reduced by half. It is therefore necessary for the position of the first null to be selected. Accordingly, the required position is found when the null is placed at the -3 dB point of the individual characteristic. It is not intended to prove this here, but this will be seen with the aid of Figure 2 :

The beamwidth of the individual antenna (Figure 2a) i.e. the angle between the points of 0.71 of the receive voltage, amounts to approximately 80° . A spacing of $D = 0.75 \lambda$ will generate zero positions at $\pm 41.8^\circ$ and limit the main beam to somewhat less than 40° as will be seen in Figure 2.

$D = \lambda/2$ (Figure 2b) will lead to a beamwidth of approximately 50° , which is unsatisfactory; $D = \lambda$ will reduce the main beam to approximately 30° , but will result in a very large side lobe (Figure 2d).

If half the beamwidth $\Theta/2$ is inserted for φ in equation (2), the following will be obtained:

$$D_{\text{opt}} = \frac{\lambda}{2 \sin \Theta/2} \quad (3)$$

There are a number of other methods of calculating the optimum spacing D_{opt} , e.g. using the gain calculation by integration of the diagram, or calculating the aperture. The result will be equally accurate and identical.

At the optimum stacking distance, the first side lobe will always be approximately 13 dB down on the main beam. Figure 2 shows how the side lobes become greater on increasing the spacing. It will also be seen clearly why the gain formula will no longer be valid with diagrams having strong side lobes, since the gain will remain constant due to the side lobe losses in spite of the fact that the main beamwidth becomes narrower.

It is interesting to see that the optimum stacking distance of even such short antennas as 3-element Yagis is greater than half a wavelength. According to the author, the stacking gain D amounts to 2 dB at 0.5λ , to 2.8 dB at $D = 0.75 \lambda$ ($\approx D_{\text{opt}}$) and fluctuates between 2.8 and 2.95 dB at larger values of D .

If the relationship between D_{opt} and the beamwidth Θ is traced, this will result in the diagram given in Figure 3, which is well known from other publications.

4. OTHER SPACINGS

It is often advisable in practice to know how a deviation from a calculated value has an effect on the gain.

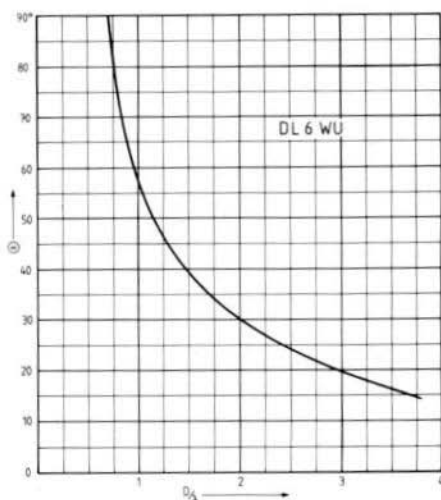


Fig. 3: Optimum stacking distance for two identical directional antennas

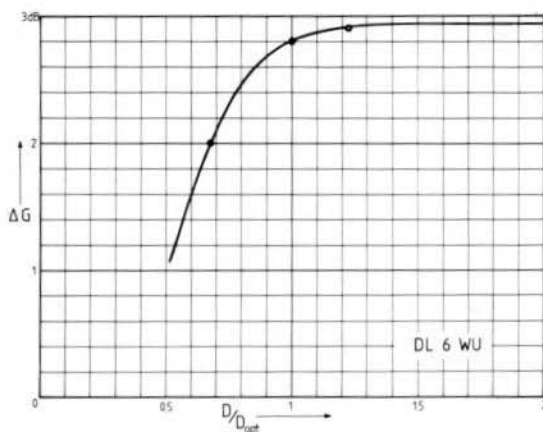


Fig. 4: Stacking gain for two antennas on deviating from the optimum spacing

If the spacing is increased, the side lobes will also increase as previously mentioned, the main beam will become sharper, but the gain will only increase by a fraction of a dB in each stacking plane. This very low increase in gain is not worthwhile when considering the given disadvantages and the expense and effort of construction, and can easily be lost in the extra length of the feeders.

The gain will fall off rapidly at spacings that are less than optimum, and the increasing coupling between the antennas will also play its part. **Figure 4** shows the mean values of numerous measured values from various sources.

It may be acceptable in many cases to reduce the spacing to 0.75 of D_{opt} ; in this case, the stacking gain will result in approximately 2 dB and virtually no additional side lobes will be generated. Obviously there is little room for compromises.

5. LARGER GROUPS

The previous example was valid for an array of two antennas. If larger groups are to be formed, it will be necessary to add further antennas in the horizontal or vertical plane, or to form a matrix. The superposition principle remains valid, and it is, for instance, possible to class the array of two stacked antennas described in section 3 as an individual antenna. If an array of four antennas has been optimally stacked, this can also be considered as an individual antenna to form even larger groups.

The geometric method pointed out in chapter 3 will give twice the spacing of the individual antennas for the center-to-center spacing of two such arrays of four antennas. This is where the values deviate slightly from another according to the different methods.

However, the gain of very large arrays (more than 16 individual antennas) will mainly be determined by the aperture, which means the actual advantage of Yagi antennas is lost more and more.

Principally speaking, approximately 2.5 dB increase of gain can be expected in practice with each doubling the antenna (7).

6. DEMANDS ON THE INDIVIDUAL ANTENNAS

When designing an antenna array, it will usually be based on a certain individual antenna. The characteristics of this antenna should be known exactly if optimum results are to be achieved.

The most important characteristic is the radiation diagram in the plane to be stacked. One requires the beamwidth (-3 dB), and the side lobe suppression. A close relationship exists between these magnitudes and the gain (8). If several different antennas having the same gain are available, the most suitable will be the one having the lowest side lobes. Since it must then have the largest beamwidth, it will require the lowest stacking distance. Required is a side lobe suppression of at least 15 dB.

This value is, unfortunately, not exhibited by most long Yagi antennas. Another difficulty is that mostly only the E-plane diagrams are available (in the polarization plane), and the side lobes in the H-plane are always considerably greater. If antennas with strong side lobes are combined to form arrays, this will result in several disadvantages:

In addition to the mechanical problems due to the unnecessarily large spacings there will be the higher pointing accuracies due to the sharper main beam. The number and magnitude of the side lobes in the overall diagram will increase due to the unavoidable side lobes of the array characteristics which are superimposed on the individual characteristic. In the case of EME arrays (large groups of antennas for moonbounce communications), this will increase the possibility of receiving additional noise and interference sources.

There are some examples of long Yagi antennas for 2 m and 70 cm having a clean polar diagram. Virtually all antennas in the 9- to 12-element class possess a sufficiently good side lobe rejection.

7. EXAMPLE

Required is an antenna for the 2 m band having a gain of approximately 18 dB over a dipole. This means that two Yagis of at least 15 dB, or four Yagis of 12 to 13 dB are to be combined to form an array.

It will be seen in Figure 1 of (6) that a 15 dB Yagi will have to be at least 5λ long, which amounts to over 10 m. This means that a group of four antennas is advisable.

In order to obtain a gain of 12.5 dB, a minimum length of 2.3λ or approximately 4.5 m is required. A 10-element antenna according to (6) of 4.5 m in length and 12 to 12.5 dB gain would meet these demands. The beamwidths would be in the order of 35° , or 40° respectively. This can be checked by placing these values in the Kraus-equation which results in a gain of 12.55 dB, an acceptable value.

The stacking distances for horizontal polarization can be calculated as follows:

$$\text{Vertical spacing } D_H = \frac{2.08 \text{ m}}{2 \times \sin 20^\circ} = 3.04 \text{ m}$$

$$\text{Horizontal spacing } D_E = \frac{2.08 \text{ m}}{2 \times \sin 17.5^\circ} = 3.46 \text{ m}$$

This antenna array exhibits a beamwidth of 17.5° horizontal and 20° vertical which corresponds to a calculated gain of 18.6 dB, from which approximately 1 dB must be subtracted for the side lobes.

This relatively compact antenna array represents the lower limit for EME communications. The gain is in excess of that of a 64- or 80-element colinear array. Model measurements on the 70 cm band have proved the calculated values; the stacking gain was measured to be 2.7 or 2.8 dB at the given spacings.

8. FEEDING

The author does not intend to discuss all possible methods of feeding the antenna groups, this has been described in detail already elsewhere (7, 9). It is important that all antennas are excited with identical amplitude and identical phase (except for some special cases). The cable lengths within the group should have a low VSWR and should be as short as possible, but of identical length. Low-loss cable should be used.

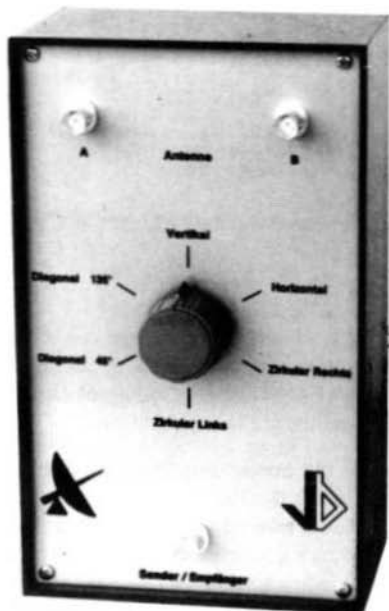
Each tenth of a dB of line loss will be added to the noise figure of the receiver or preamplifier, which in the ideal case would be located at the interconnection point of the feed.

It is advisable for such practice to be taken into consideration, especially with the low-noise transistors available today, otherwise all the effort and difficulties will not have been worthwhile.

The old proverb that »a good antenna is the best RF amplifier« still remains valid, even when used in conjunction with the best preamplifier.

9. REFERENCES

- (1) C. Greenblum: Notes on the Development of Yagi Arrays
Part II: Stacking Yagis
QST, September 1956, pages 23-26, and 122
- (2) H.W. Kasper: Optimum Stacking Spacings in Antenna Arrays
QST, April 1958, pages 40-43
- (3) H.W. Kasper: Array Design with Optimum Antenna Spacing
QST, November 1960, pages 23-26
- (4) T. Bittan: Antenna Notebook
VHF COMMUNICATIONS 6, Edition 2/1974, pages 82-84
- (5) J.F. Kraus: Antennas
McGraw-Hill, New York, NY
- (6) G. Hoch: More Gain with Yagi Antennas
VHF COMMUNICATIONS 9, Edition 4/1977, pages 204-211
- (7) Almost everything you want to know about moonbounce
AS 49, EIMAC Div. of VARIAN, San Carlos, CA
- (8) G. Hoch: Operation and Optimum Dimensions of Yagi Antennas
VHF COMMUNICATIONS 9, Edition 4/1977, pages 204-211
- (9) H.S. Brier and W.I. Orr: VHF Handbook for Radio Amateurs
Radio Publications, Wilton, CT



NEW! NEW! Polarisations Switching Unit for 2 m Crossed Yagis

Ready-to-operate as described in VHF COMMUNICATIONS. Complete in cabinet with three BNC connectors. Especially designed for use with crossed yagis mounted as an »X«, and fed with equal-length feeders. Following six polarisations can be selected: Vertical, horizontal, clockwise circular, anticlockwise circular, slant 45° and slant 135°.

VSWR:	max. 1.2
Power:	100 W carrier
Insertion loss:	0.1 to 0.3 dB
Phase error:	approx. 1°
Dimensions:	216 x 132 x 80 mm

UKW-TECHNIK · Hans Dohlus oHG · D-8523 BAIERSDORF

A 20 W POWER AMPLIFIER WITH INTEGRATED PA-MODULE FOR FM TRANSCEIVERS ON THE 2 m BAND

by J. Becker, DJ 8 IL

For many years now, transistorized transmitters for the frequency range of 2 to 500 MHz with power levels from 0.1 to 100 W have been constructed according to the same basic circuit principles. It seems that a certain technical optimum has been reached, and the next logical step seems to be the integration into a small black box, by which many alignment elements are deleted.

Such black boxes firstly appeared on the market in the USA as power amplifiers for UHF transceivers, since the internal matching networks could easily be realized in the form of striplines. Such modules are now also available for the VHF-range: A hybrid amplifier series manufactured by Philips (1) covers the frequency range from 68 to 174 MHz in four pass bands. The matching elements (**Figure 1**) consist of chip capacitors and printed inductances. Input and output impedance are a real 50Ω during nominal operation. The dimensions of the modules are 67.5 mm x 19.7 mm x 8 mm. At an operating voltage of 12.5 V and an input power of 150 mW, these modules will provide an output power of at least 18 W.

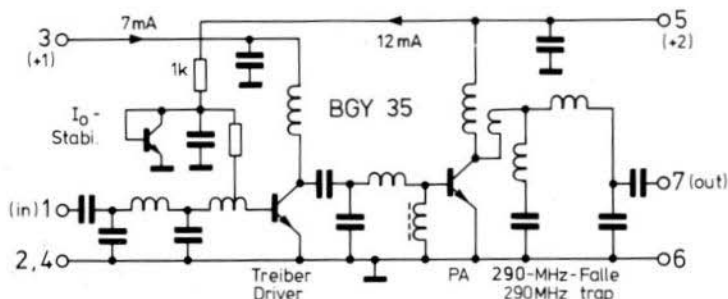


Fig. 1: Internal circuit of the hybrid integrated VHF amplifier BGY 35 / BGY 36

1. CONCEPT

This article is to describe what is necessary for the radio amateur to consider in conjunction with these modules: Sufficient rejection of the harmonics and unwanted spurious signals from the exciter, and provision of a reliable low-loss VHF-VOX. Several different circuits are to be given for the VHF-VOX-circuit, and their characteristics are to be described.

Table 1 contains the most important specifications of the power amplifier, which has been designed for use with the SUEWIND hand-held transceiver (2). The overall circuit is given in **Figure 2**, and the output spectrum at the antenna socket is given in **Figure 3**. It is possible to connect all FM transceivers without loss of output whose power output is at least 0.25 W. Only the values of several components in the input network should be coarsely matched to the various drive power levels. The amplifier module itself is able to handle a maximum input power of 0.3 W.

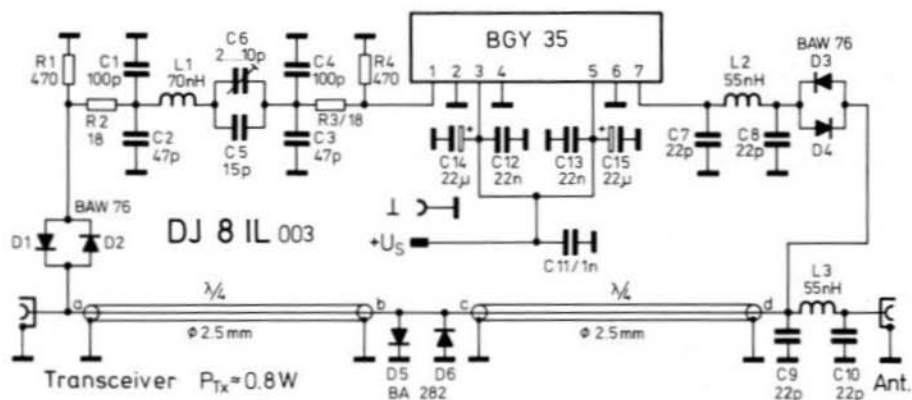


Fig. 2: Circuit diagram of the power amplifier

Table 1: Specifications, mean values of three such modules

Output power:	17 W at 12.5 V
Efficiency:	52 % (including SUEDWIND: 47 %)
Harmonic output, max.:	- 62 dB
Spurious radiation, max.:	- 61 dB (with - 44 dB from the transceiver)
Quiescent current:	19 mA
Insertion loss (Rx):	0.5 dB
Exciter: SUEDWIND with P_{tx} :	$= 0.9 W/f = 145.25 \text{ MHz} \triangleq \text{channel } 50$

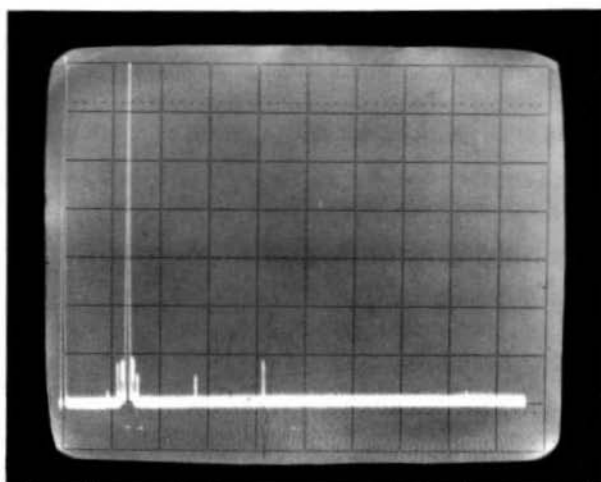


Fig. 3: Transmit spectrum, measured at the antenna socket with HP 180 A + 8558 B, and using the SUEDWIND as exciter;
 hor.: 0-1 GHz (100 MHz/Div.), vertical: 10 dB/Div.
 $f = 145.25 \text{ MHz}$; SUEDWIND-spurious level: max. - 44 dB

1.1. Input filter

In order to ensure stable operation of the amplifier module under differing drive conditions, the manufacturer recommends an isolating link having at least 1.5 dB to be placed in the input line. In Figure 2, this Pi-attenuator (R 1 to R 4) is disconnected at the center and extended using a resonant circuit (L 1, C 1 to C 6), which attenuates the spurious and harmonic signals from the exciter.

Crystal-controlled transceivers often show a whole spectrum of sidelines spaced $\pm n \times f_Q$ from the carrier frequency. In the case of transmitters with superhet frequency processing, sidelines spaced to the value of the intermediate frequency are usually the strongest. The interference lines should not be greater than -46 dB at an output power of 1 W, and should not be greater than -60 dB at high power levels.

This means that a minimum Q of $Q_B = 34.5$ was calculated for a single-stage filter. The upper limit of Q_B is limited due to the required bandwidth that the transmitter should be able to cover without power drop-off, as well as the maximum reactive power at resonance that can be handled by the components. The latter is the reason for the rather extensive Pi-circuit with the series resonant circuit in the longitudinal branch: The operating Q $Q_B = P_b/P_w$ results in approximately two equal parts from the relationship: reactive current in the resonant circuit to transferred required current and reactive voltage via C 5 and C 6 to the required voltage at the input points (R 2, R 3). The 180° phase reversal of this Pi-network is of advantage for the stability when operating in conjunction with an electronic VHF-VOX.

The following specifications were found after trimming for max. output power at 145 MHz:

Attenuation: 7.0 dB (nominal value: $0.85 \text{ W}/0.15 \text{ W} = 7.5 \text{ dB}$), $R_{in} \approx 52 \Omega$

- 3 dB bandwidth: 3.55 MHz $\rightarrow Q_B = 41$

Power drop at the band limits: < 0.2 dB

The power loss at the band limits is so low because the amplifier module operates in the saturation range of the P_o/P_i characteristic. A comparison of the output spectrum (Figure 3) to the input spectrum shows an approximately 3 dB higher interference level in the vicinity of the carrier than in Fig. 26 of (3) and demonstrates the efficiency of this simple filter.

The spectral specifications given in Table 1 and Figure 3 are valid at least for the FM-range from 145.0 to 145.5 MHz, whereas it will be a few dB more at the band limits of the 2 m band.

1.2. Output Filter

The amplifier module produced the following harmonic spectrum at the output:

2 f	3 f	4 f	5 f	6 f	
- 34 dB	- 56 dB	- 40 dB	- 54 dB	- 59 dB	f = 145 MHz

A 2-stage Pi-filter of conventional design $2 \pi f L = 1/2 \pi f C = 50 \Omega$ would have 32 dB at 2 f, and 55 dB at 3 f, which means that it should be sufficient to clean up this spectrum.

2. ANTENNA CHANGEOVER SWITCHING

In the receive mode, it is necessary for the transmit amplifier to be bypassed in a low-loss manner. Five different methods of RF-controlled changeover switching (VHF-VOX) were examined in order to gain experience in this type of circuitry.

Figure 4 a shows the classical method using 2 relay contacts (3). When using suitable relays, this circuit can be used up to the GHz-range and is suitable for all power levels. Switch S is to disable the VHF-VOX when the power amplifier is not required. In the receive mode, losses will be caused by the two relays, and in line l. This will be in the order of 0.35 dB.

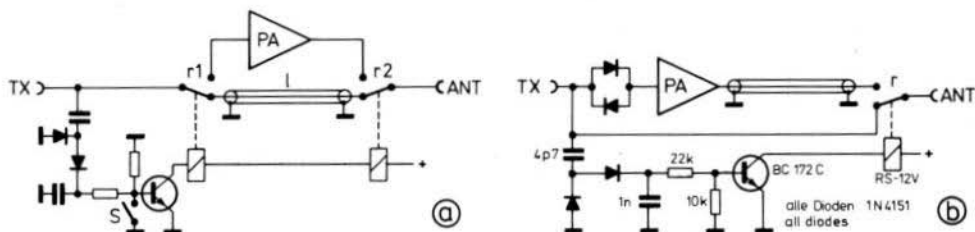


Fig. 4: VHF-VOX circuits with relays. In Fig. 4 b, the coaxial sockets for Tx and antenna are in the direct vicinity of the relay

The circuit given in **Figure 4 b** is recommended by the author in order to obtain the lowest possible loss in the receive branch: In excess of approximately 100 mW input power, it is possible for relay r₁ to be replaced by fast switching diodes when the power amplifier is to remain in circuit at all times. An insertion loss of 0.15 dB was measured in the receive branch when using an inexpensive National RS-type relay.

In the purely electronic circuits given in **Figure 5**, the exciter power is fed to the amplifier via the anti-phase diodes D 1, and D 2, and the amplified VHF signal also fed via a further pair of anti-phase diodes (D 3 and D 4) to the antenna. All diodes are blocked in the receive mode since the receive signal is practically always below their conducting threshold. They should have a low junction capacitance at 0 V.

Diode D 5 and D 6 in the receive signal path will conduct in the transmit mode, and form a VHF-shortcircuit to ground. This means that the series resonant circuit L, and C in **Figure 5a**, or the $\lambda/2$ line in **5b** and **5c** will be disconnected. The amplifier given in Figure 5a will become capacitive at the input due to C, and the output will be inductively detuned by L. For this reason, this simple circuit (4) can only be used with amplifiers constructed from discrete components, where the reactive components can be taken into consideration during the alignment.

In Figures 5b and 5c, on the other hand, the amplifier will not be detuned: the bypass branch will form two $\lambda/4$ circuits during transmit which will represent an open circuit under ideal conditions at the other end, and will therefore be completely decoupled (5). The reactive current in the right-hand $\lambda/4$ circuit maintains diodes D 5 and D 6 in their flow range. These diodes should possess a sufficiently long carrier lifetime similar to PIN diodes. The cheapest solution is to use switching diodes as used in TV-tuners. The insertion loss of the receive branch in circuit 5b amounts to 0.4 dB.

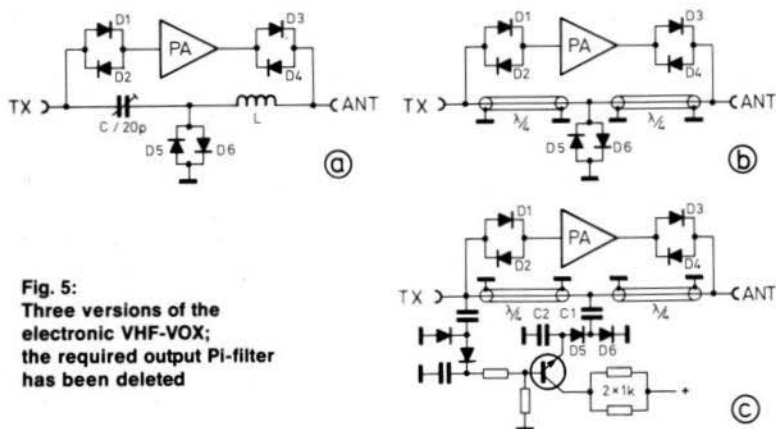


Fig. 5:
Three versions of the
electronic VHF-VOX;
the required output Pi-filter
has been deleted

As in the case of electronic duplexers (6), somewhat better characteristics are to be expected if D 5 and D 6 are biased with an additional DC-current in the transmit mode (Figure 5c). The required rectifying amplifier is similar to that used for relay control in Figure 4b. Measurements made on two boards constructed according to 5b and 5c exhibited the following characteristics:

A hardly noticeable increase in output power was gained, and the second harmonic was somewhat weaker (< 3 dB), however, the spurious rejection was somewhat less than without bias current. Parasitic oscillation at $f/2$ and $3/2 f$ appeared in the spectrum when capacitors were used for C 1 and C 2 that had a non-linear dielectric (type 2) (470-2200 pF), especially when C 2 was greater than C 1. A bias current of 20 to 30 mA through the diode type BA 282 was not sufficiently great for the VHF drive to be classed as a low-signal level; this was proved by the drop of the DC-voltage across D 6 from 0.8 V without VHF to 0.3 V in the transmit mode; this shows that DC-biasing is not suitable. Further specifications for the circuit given in 5b measured in conjunction with a completed amplifier according to the circuit given in Fig. 2, are listed in **Table 2**.

Table 2: Further specifications, comparison of three modules

Losses in the output Pi-Filter:	0.3 dB
Losses in the output coupling diodes (D 3, D 4):	0.15 dB
Losses due to the VHF-VOX line:	0.1 dB

Module	Output filter and VHF-VOX				
	without I_S	without P_o	with I_S	with P_o	with η
437 BGY/L	3.50 A	22.4 W	3.0 A	18.6 W	50 %
BGY 36-SA 64	3.10 A	19.0 W	2.5 A	16.3 W	52 %
BGY 36-SA 65	3.05 A	19.6 W	2.4 A	16.5 W	55 %

$U_S = 12.5$ V $P_i = 0.9$ W $f = 145.25$ MHz

3. COMPONENT LIST

BGY 35/BGY 36:	Mullard (Philips)
C 1 - C 5:	Ceramic 1 b, type EDPU/63 V (Philips)
C 6:	Plastic foil trimmer 7.5 mm dia., Philips-2222 808 11109 (yellow)
C 7 - C 10:	Ceramic 1 b, 8 mm dia., TC = N 150, type SDPN (Draloric), $\leq 5\%$
C 11 - C 13:	Ceramic 2, type EDPU/40 V (Philips)
C 14 - C 15:	Electrolytic 22 μF / 25 V
R 1 - R 4:	Spacing 10 mm
L 1:	5 turns, inner dia. 4 mm, 7 mm long
L 2, L 3:	4 turns, inner dia. 5 mm, 7 mm long
	* air-spaced coils from 1 mm dia., silver-plated copper wire, pay attention to direction of winding ! (Fig. 8)
D 1, D 4:	Fast switching diodes BAW 76 (Siemens)
D 5, D 6:	Switching diodes from TV-tuners BA 282
VHF-VOX receive line:	2 x 35 cm RG-174 U ($\lambda/4$ x VF)

4. CONSTRUCTION DETAILS

The heat sink is used as case. Further preparations are shown in **Figure 6**.

The components are mounted on the conductor side of the 134 mm x 34.5 mm large board DJ 8 IL 003. The diodes and resistors are directly mounted onto the board, and the three

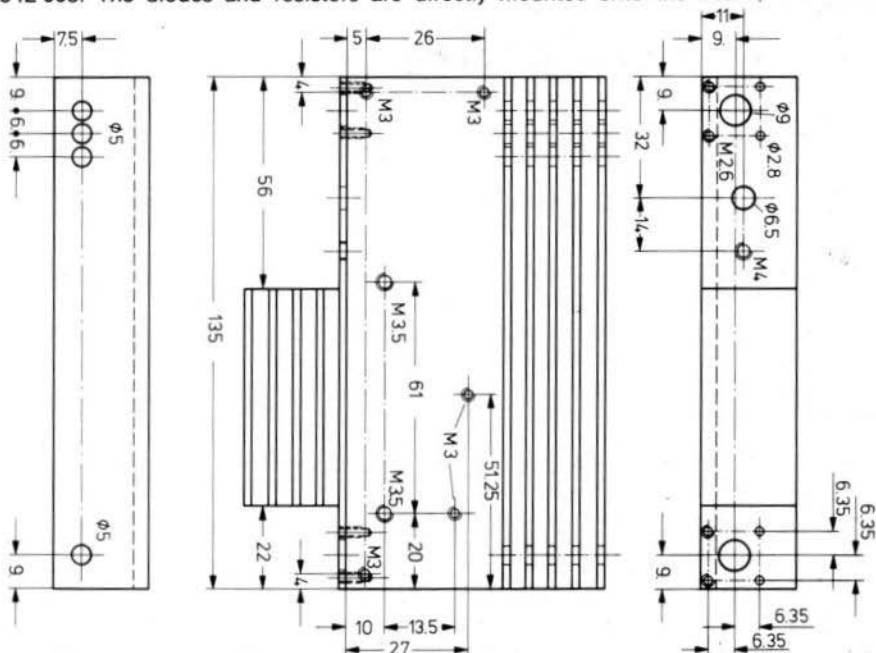


Fig. 6: Preparation of the heat sink/case;

Heat sink: Fischer SK 04 SA, 135 mm long

Accessories: 5 nuts M 3, threading drilled out; 5 screws M 3 x 8 (cylinder head)

4 nuts M 2.6; 8 screws M 2.6 x 6 mm (cylinder head); 2 screws M 3.5 x 7 mm (cylinder head)

inductances are soldered into place with a spacing of 1.5 mm from the board. All capacitors should be installed with the shortest possible leads. Large ceramic disk capacitors of 8 mm diameter are used in the output filter (C 7 to C 10), because the usual miniature types EDPU are not suitable due to the high reactive load at this position; they would then generate harmonics, especially the third harmonic. For instance, the 3 f-level was measured to be - 51 dB and - 67 dB for the two capacitor types.

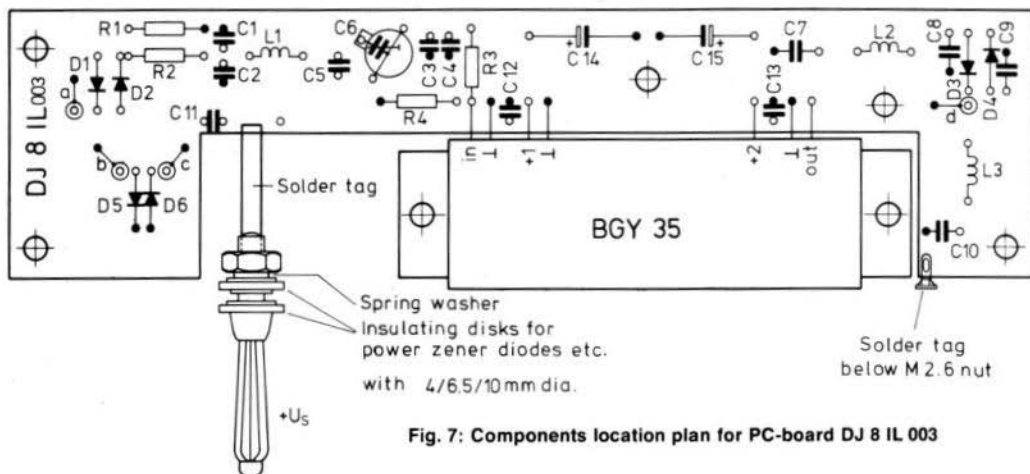


Fig. 7: Components location plan for PC-board DJ 8 IL 003

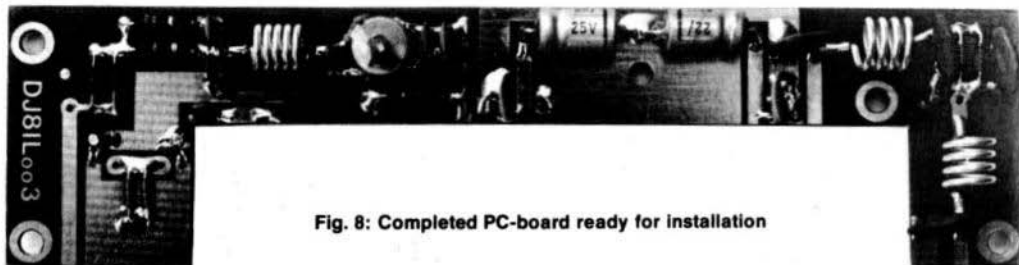


Fig. 8: Completed PC-board ready for installation

In the components location plan given in **Figure 7**, a bent solder tag is used as additional ground connection from C 10 to the antenna connector. This tag should not be forgotten during assembly, since it provides a better suppression of the higher harmonics. If a through-contacted PC-board is not available, it is necessary for all ground connections to be made at both sides of the board. Four solder pins are provided for connection of the outer conductors on both ends of the $\lambda/4$ cables.

The diodes used are high-temperature, pressure-contact types (double heat sink technology). These diodes can be soldered right up to the vicinity of the glass case in order to keep the inductivity as low as possible, which is especially advisable in the case of D 5 and D 6.

The components are located on the board as shown in **Figure 8**, after which it is screwed to the heat sink with the aid of five screws. Five M 3 nuts are drilled out and used as spacers. The BNC-connectors, the solder tag of the $+U_S$ -plug and the previously mentioned ground tag are now soldered into place. This is followed by inserting the two 35 cm coaxial cables (**Figure 9**). The exact dimension of these cables is 34.1 cm; however, a deviation from the electrical characteristics will not be noticed until the deviation is greater than 2 cm.

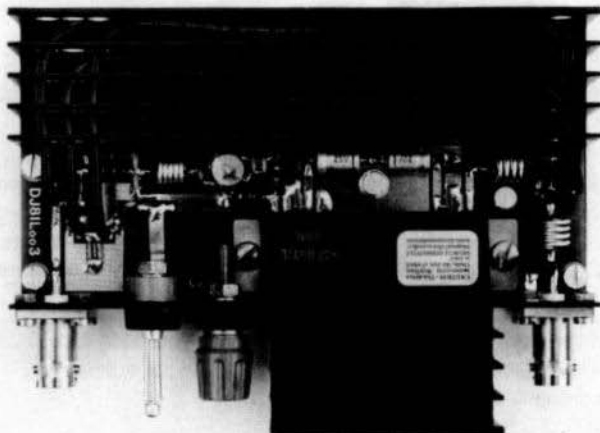


Fig. 9: Photograph of the completed amplifier

Finally, the actual amplifier module is mounted into place. Its connection leads should be previously shortened down to approximately 3 mm in length and the lower surface thinly coated with heat-conductive paste. The components can be protected using a 1.5 mm thick aluminium plate placed in the groove of the two inner ribs of the heat sink. No noticeable change of the spectrum will occur under these conditions which indicates that it is not necessary for any screening measures to be made if the layout of the board is favorable.

5. ALIGNMENT

The power amplifier is constructed as a plug-in module, and protected against incorrect polarity. It is best to feed the plus-cable (4 mm²) direct to the car battery and the ground cable to the nearest ground point. No filter measures were required. For alignment, C 6 is trimmed for maximum current drain. This adjustment also gives maximum output power and maximum spurious rejection. A slight increase of output power could be obtained by exact matching of the output filter to the amplifier module. This is achieved by placing an additional capacitance of several pF in parallel to C 7 or C 8.

6. REFERENCES

- (1) P. J. Hart: Transmitter Design with VHF Broadband Amplifier Modules
Application note, Mullard Ltd., Mullard House, Torrington Place, London WC 1 E 7 HD
- (2) J. Becker: SUEDWIND – A 2 m-FM Hand-held Transceiver with 80 or 396 Channel
Synthesizer and Touch-Key Operation – Part 1: Circuit Description
VHF COMMUNICATIONS 10, Edition 4/1978, pages 194-212
- (3) G. Otto: A 144 MHz Linear Amplifier with 25 W Output at 12 V to 14 V
VHF COMMUNICATIONS 5, Edition 2/1973, pages 81-90
- (4) F. Kühne: Drake-Endstufe AA 10 – Funkschau 46 (1974), page 848
- (5) Heath – Power Amplifier HA 201
- (6) M. J. Köppen: Electronic Antenna Switches for the 160 MHz Band Using BA 182 Diodes
Application Report ECO 6918, Philips

QUADRATURE DEMODULATORS

by A. Meier, DC 7 MA

Coincidence or quadrature detectors are demodulators suitable for frequency modulation (FM); such demodulators have become popular together with the integrated IF-amplifiers/demodulators such as types TBA 120 or CA 3089. This article is not to discuss the theory of operation, but more to discuss practical experiences using such demodulators. The following descriptions used such demodulators:

- (1) FM-IF module of the DC 6 HL transceiver – DC 6 HL 007 with TBA 120
- (2) FM-IF module in the TEKO set system – DK 1 PN 005 with CA 3089 E
- (3) FM-broadcast receiver – DK 1 OF 021 with TBA 120
- (4) FM-transceiver RT-33 – DC 3 NT 001 with TBA 120
- (5) ULM-70 – DJ 0 FW 001 with CA 3089 E
- (6) Hand-held transceiver SUEDWIND – DJ 8 IL 001 with TDA 1047
- (7) 2 m FM receiver – DK 1 OF 034 with CA 3089 E

Hardly any difficulties are encountered when using quadrature demodulators for wideband FM, as long as the manufacturer's recommendations are followed. A squelch circuit can also be realized easily, since a wideband noise will be present from which any required frequency can be filtered out for the squelch circuit. As can be seen in **Figure 1**, the demodulated AF-voltage at a frequency deviation of ± 100 kHz is virtually as great as the noise voltage.

It is, however, more difficult when using the circuit in the narrow-band FM mode used for communications. The reason for this is that the phase-shift, or reference resonant circuit at the demodulator is too wideband with respect to the frequency deviation used. The phase-shift across the resonant circuit which is necessary for demodulation is very low. One possibility of solving this problem is to use a lower intermediate frequency, e.g. 455 kHz. The relationship of frequency deviation to bandwidth of the resonant circuit will then be sufficiently great even when using resonant circuits of moderate Q. This solution has, however, technical disadvantages, which means that it is not generally used.

On the other hand, if the quadrature demodulator is used at a higher IF (9 MHz, 10.7 MHz or even 21.4 MHz), the ratio of frequency deviation to bandwidth of the phase-shift circuit will be small and the reclaimed AF will be low. This is indicated in **Figure 2** for a frequency deviation of ± 7.5 kHz. The 15 kHz filter also only allows a small amount of noise to pass, which means that the squelch will also not operate correctly. Either it will not open or, if it opens, will be closed again at moderate frequency deviation levels which occur during voice modulation.

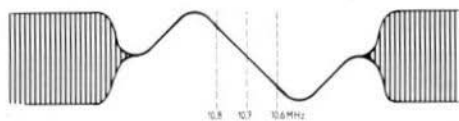


Fig. 1: Wideband operation

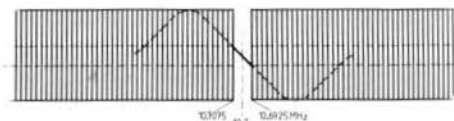


Fig. 2: Narrow-band operation

In order to avoid these problems, it is necessary for a high-Q phase-shift circuit to be used (2), (5). The results given in **Figure 3** are then valid.

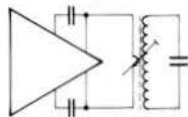
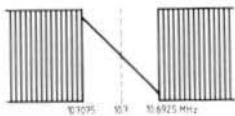


Fig. 3 and 4: High-Q phase-shift circuit for narrow-band FM

Since it is usually inductances that are responsible for the Q of the resonant circuit, it is necessary for further measures to be taken here. Higher Q-values can be obtained using potted cores, or toroids made from a suitable material – this method was used in (2). The correct L/C ratio and coupling is also important. Even the highest Q of the resonant circuit is useless when too tightly coupled. Of course, this is not new, however, the author has still not seen a quadrature demodulator having an extremely loose coupling to the phase-shift circuit. An experiment made in this direction was surprisingly successful (**Figure 4** shows a circuit of such a demodulator with only one coupling turn):

The demodulator characteristic when using such loose coupling provided such a high Q and was so narrow that it was necessary to connect a resistor in parallel to reduce the Q. When this resistor was deleted, the reproduction was distorted or even unintelligible, since the demodulation characteristic was utilized in excess of the humps (**Figure 5**).

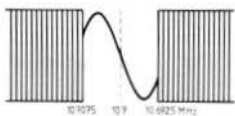


Fig. 5: A hump spacing that is too low

Even better results were obtained when using a low-Q resonant circuit for the demodulator and providing an additional crystal whose resonant frequency is at the center of the demodulation characteristic, i.e. at 9.0 MHz, 10.70 MHz or 21.40 MHz (in order to use the standard center frequencies of available crystal filters). The circuit given in **Figure 6a** was extremely successful. It may even be necessary for the Q to be reduced somewhat with the aid of a parallel resistor.

With a loose coupling of the resonant circuit and crystal, on the other hand, such a sharp resonance of the reference circuit will result, as can be seen in **Figure 6 b**, that the circuit can break into oscillation. In this case, an unsatisfactory demodulation characteristic will result as shown in **Figure 7**.

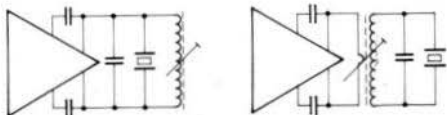


Fig. 6: Circuits using additional crystals

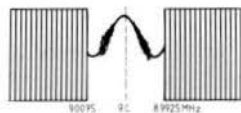


Fig. 7: Oscillation effects

After studying the results of this, a crystal was used in the circuit shown in Figure 6 b, whose resonant frequency was outside of the passband range of the filter. The result was the demodulation characteristic shown in **Figure 8**. The slight curvature originates from the slope of the crystal resonant curve; this causes a very slight distortion of the demodulated signal, however, this is hardly noticeable for voice communications.

A CB-crystal for the 11 m band with a nominal frequency of 27.045 MHz was used for the last experiment. The fundamental frequency of this crystal was 9.015 MHz. This means that its resonance was 15 kHz from the center frequency, or approximately 7 kHz from the corner frequency of the filter. No spurious reception points or other interference was noticed.

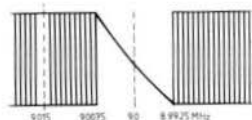


Fig. 8:
Characteristic curve when using a crystal resonator frequency outside of the passband range of the filter

All described experiments were made in conjunction with a crystal filter type XF-9 E in the IF-amplifier, using the previously mentioned IF-amplifier/demodulator types. All integrated circuits exhibited the same behaviour in conjunction with the different reference circuits.

When using a circuit as shown in Figure 6 b, the squelch of the ULM-70 receiver operated correctly even without the additional circuitry (5).

One will often see the circuit shown in **Figure 9 a**, where the phase-shift is made with the aid of a capacitor. If one observes the noise voltage by connecting an oscilloscope to connection 7, it will be seen that the center is asymmetric. When using a choke of approximately 22 μ H instead of the capacitor (**Figure 9 b**) this effect will be avoided, and the squelch will operate correctly.

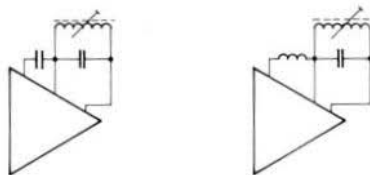


Fig. 9: Phase-shift using a capacitor or inductance

It has been said that the integrated circuits CA 3089 E and TDA 1200 break into oscillation easily. For this reason, a few tips are to be given here. The main fault is that the signal is injected at high impedance. The data sheets indicate, however, that the input should »see« 50 Ω . If this is taken into consideration, and the bypass capacitors for connections 3 and 11 are not too far away from the IC (max. 5 mm), these circuits will operate to 99 % without tendency to oscillation. In addition to the information given by the manufacturer it is also possible to bypass connections 13 (S-meter) and 15 (AGC) to ground (connection 14) using ceramic 1 nF capacitors. These connections should be as short as possible, if possible, direct at the IC.

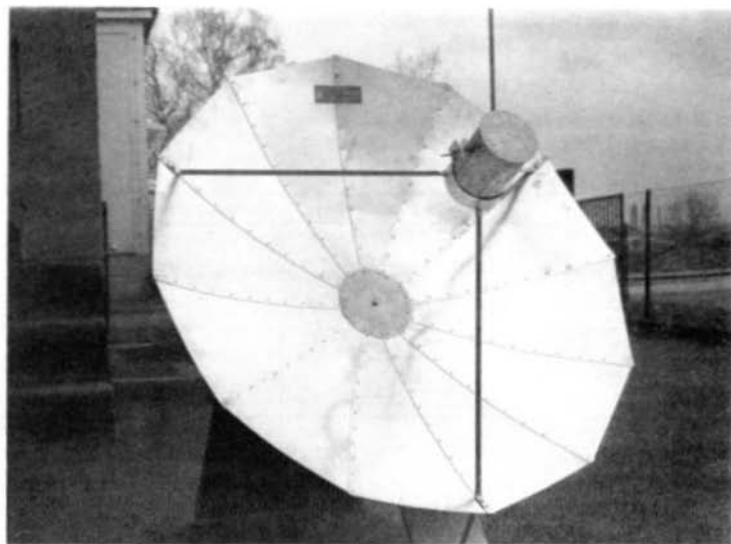
Experiments were made using the following IC-types:

- TBA 120 (ITT-Intermetall)
- TBA 120-S (various manufacturers)
- SO 41 P (Siemens)
- CA 3089 E (RCA)
- TDA 1200 (Signetics)
- SN 76622 N (Texas Instruments)

The following measuring equipment was available for the measurements:

- Oscilloscope Hameg 312/5
- Two-channel plug-in
- Swept frequency generator from DC 7 LE
- Frequency counter
- Variable attenuator (2 to 90 dB)
- IF-amplifier with crystal filter XF-9 E

Of course, the described experiments were not able to cover all possibilities, and the results are not designed to indicate that all previously described circuits are inefficient. The author hopes that his experiments will give »food for thought« so that further experiments will be made using this type of FM demodulator.



NEW! 1.2 m Parabolic Dish. Available complete with radiator or as kit. Suitable for use between 1 GHz and 3 GHz. Construction to be described in the next edition of VHF COMMUNICATIONS. Kit to include tools for construction of the dish; with all parts cut to size and necessary holes drilled. Price and further details on request.

UKW-TECHNIK · Hans Dohlus oHG · D-8523 BAIERSDORF

DESIGN OF CRYSTAL OSCILLATOR CIRCUITS

by B. Neubig, DK 1 AG

1. PRINCIPLE CONSIDERATIONS

1.1. Crystal Oscillators Using Low-Frequency Crystals

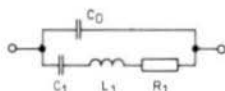
All flexure, extensional and face-shear mode vibrators, whose resonant frequency is typically less than 1 MHz are to be designated here as LF-crystals. This means that thickness-shear vibrators will not fall under this definition. Due to their sensitivity to mechanical shock, their large frequency-to-temperature characteristic and their higher price due to the complicated manufacture, the importance of this type of vibrator has dropped off considerably. The possibility of obtaining low frequencies with the aid of integrated (CMOS) dividers in conjunction with thickness-shear vibrators (AT-crystals) has also had its effect.


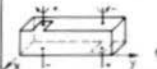
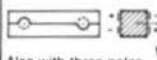
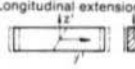
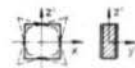
Table 1 gives a list of the most common types of vibrators in this frequency range. The temperature response of the resonant frequency is either straight or in the form of a second order parabola

$$\frac{\Delta f}{f} = -a (T - T_{inv})^2 \quad (1)$$

with a coefficient a of between $2 \times 10^{-8}/\text{deg}^2$ and $5 \times 10^{-8}/\text{deg}^2$ ($\frac{\Delta f}{f}$ in ppm $\triangleq 10^{-6}$) according to type. The inversion point T_{inv} can be varied for each vibrator by changing the design of the crystal.

Table 1: List of the most common non-AT crystals in the range < 1 MHz



Frequency Range	Vibrator Type	Mode of Oscillation	Temperature Response	R_1 [k Ω]	C_1 [fF]
800 Hz – 4 kHz	Duplex flexure vibrator	Bimetal principle 	Parabola $T_{inv} = 15^\circ\text{C}$	750 – 250	250 – 50
4 kHz – 15 kHz	X-Y flexure vibrator		Parabola $T_{inv} = +10^\circ$ to 40°C	200 – 80	50 – 15
15 kHz – 50 kHz	H-flexure vibrator	 Also with three poles	Straight -7 to -15 ppm/deg	20 – 8	35 – 20
50 kHz – 200 kHz	X + 5° extensional vibrator (e.g. 100 kHz standard crystal)	Longitudinal extension 	Parabola (16° to 55°)	4	60 – 30
200 kHz – 400 kHz 300 kHz – 800 kHz 000 kHz – 800 kHz	Face-shear vibrator DT-cut CT-cut SL-cut	 SL: rectangular	Parabola, $T_{inv} = 0$ to 60°C typ. 15°C	1– 5	30 – 7

The resonance resistance R_1 is the most important magnitude for designing crystal oscillators. This resistance at series resonance is in the order of about 1 M Ω down to 1 k Ω , which means that it varies according to the cut and frequency range by a factor of nearly 1000. This means that it is not possible to provide a standard crystal oscillator circuit for the whole range.

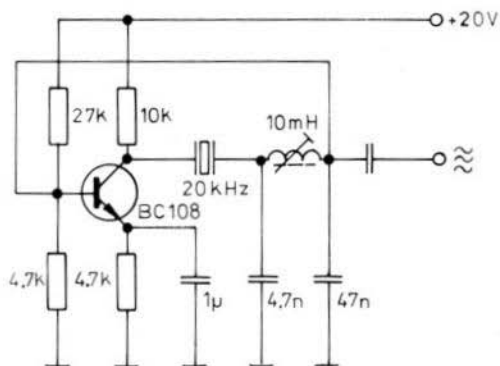


Fig. 1:
20 kHz crystal oscillator
with impedance
transformation

At large values of R_1 , it is necessary for the amplifier stage to possess a high input impedance. This can be achieved, as shown in **Figure 1**, by using impedance transformation (1). If this is not the case, it is necessary for the voltage-divider loss (crystal - R_1 : Input impedance) to be compensated for using a high loop gain, e.g. by using a two-stage amplifier as shown in **Figure 2** (2). A RC-lowpass filter is connected in the feedback link in series with the crystal. This ensures that no tendency for excitation of parasitic modes can take place, which is very prevalent with LF-crystals.

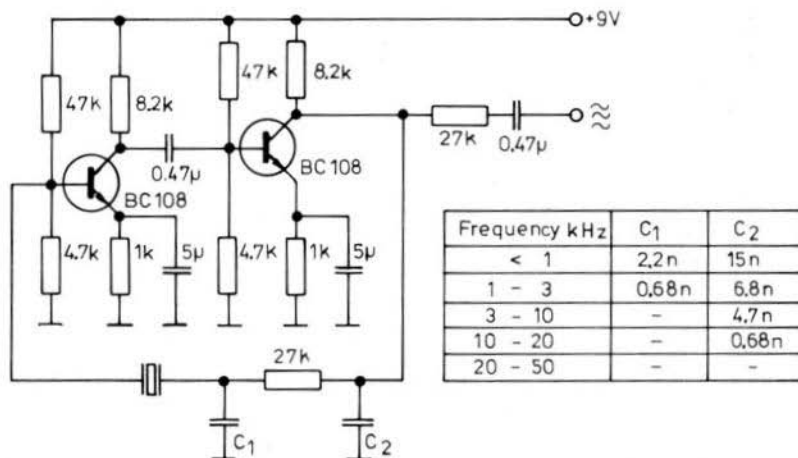


Fig. 2: Two-stage series-resonance oscillator for 0.8 to 50 kHz

The Butler-circuit as shown in **Figure 3** has proved itself well for frequencies in excess of approximately 50 kHz. If the loop gain is not sufficient, the collector resistor should be replaced by a choke or resonant circuit.

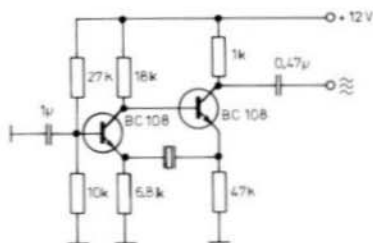


Fig. 3:
Butler-oscillator
for 50 to 500 kHz

1.2. Crystal Oscillators Equipped with Fundamental Mode AT-Cut Crystals

The most popular crystal cut is the AT-cut. AT-crystals are thickness-shear vibrators. They cover a fundamental frequency range from approximately 750 kHz to 20 MHz (and some exceptions from 500 kHz to 30 MHz).

Table 2 gives the frequency ranges of the various different crystal shapes together with their typical equivalent data ($1 \text{ fF} = 10^{-3} \text{ pF}$) which are necessary for physical reasons. The temperature response is a third order parabola whose form can be influenced by selection of the cutting angle. It is given in ppm.

$$\frac{\Delta f}{f} = a_1 (T - T_{\text{inv}}) + a_3 (T - T_{\text{inv}})^3 \quad (2)$$

where the coefficients are:

$$a_1 \approx -0.084 \times \Delta\varphi$$

$$a_3 \approx 10^{-4}$$

The inversion temperature T_{inv} is in the order of 22 to 33°C according to the range. $\Delta\varphi = \varphi_0 - \varphi$ is the angular difference (in minutes of arc) to the so-called zero TC angle φ_0 (at this cut angle the temperature coefficient will be zero at the inversion point).

As will be seen in Table 2, the typical resonance resistance R_1 will be between 10 and 500 Ω and decreases with increasing frequency.

Table 2: Equivalent Data of AT-fundamental crystals



Shape of Crystal	Frequency range (MHz) for cases			Typical Equivalent Data			
	HC-6/U	HC-25/U	HC-35/HC-45	C_0	C_1	Q	R_1
Biconvex	0.75 - 1.5	—	—	3 - 7 pF	8 fF	> 100 000	100 Ω - 500 Ω
Planconvex	1.5 - 3	2.7 - 5.2	—	4 - 7 pF	10 fF	> 100 000	< 200 Ω
Planoparallel with bevel	2 - 7	4.5 - 10.5	10 - 13	5 - 7 pF	20 fF [10 fF]	> 50 000	10 Ω - 100 Ω
Plane	7 - 20 (30)	10.5 - 20(30)	13 - 20 (30)				

The most common type of circuit for fundamental AT-crystals are aperiodic oscillators, that is oscillators without additional selectivity. The most important types of parallel-resonant oscillators are Pierce, Colpitts and Clapp oscillators that can be derived from a circuit by varying the ground point (**Figure 4**). The crystal operates at a point where it exhibits the same characteristic as a high Q inductance.

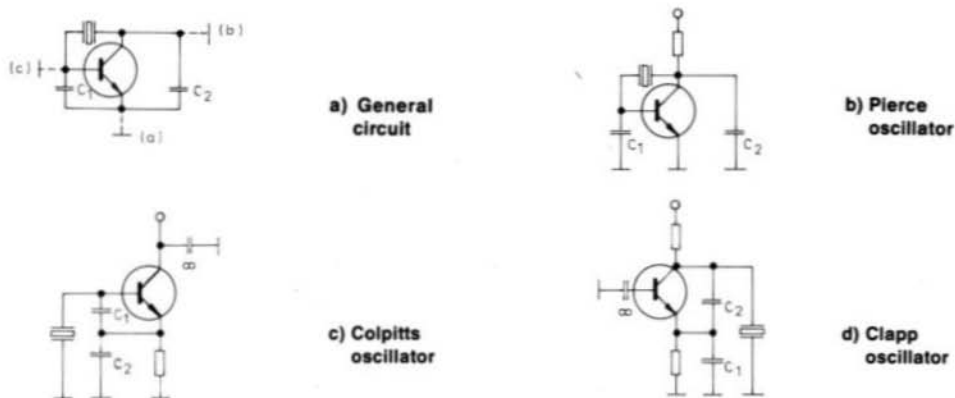


Fig. 4: Parallel-resonance oscillators for fundamental crystals (RF equivalent diagram)

A circuit equipped with a Darlington stage is shown in **Figure 5** as an example of the successful Colpitts oscillator. Due to the high input impedance, it is possible for the divider capacitors C_1 and C_2 to possess large capacitance values. This means that the reaction of the transistor stage on the oscillator frequency is very low. The effective load capacitance of the crystal is represented by the series connection of C_1 and C_2 . In order to obtain suitable standard values of approximately 30 pF (typical range 10 pF to 50 pF), an additional capacitance of this order should be placed in series with the crystal in practice in order to align the crystal frequency.

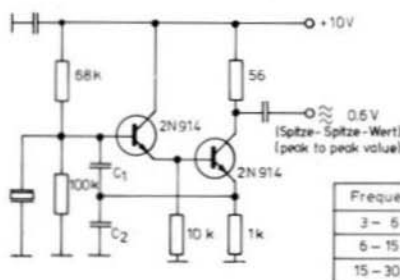


Fig. 5: Colpitts oscillator with Darlington stage suitable for fundamental crystals

Frequency	C_1	C_2
3 - 5 MHz	560 pF	470 pF
6 - 15 MHz	560 pF	220 pF
15 - 30 MHz	220 pF	100 pF

A disadvantage of aperiodic oscillator circuits is the tendency to oscillate at the third or higher overtone of the crystal, or to a non-harmonic spurious resonance. In difficult cases, capacitance C_2 should be replaced by a resonant circuit, which is detuned so that it is capacitive at the nominal frequency (principle of the Tritet oscillator).

Generally speaking, the positive feedback should not be greater than required for starting and maintaining stable oscillation. In the case of the Colpitts circuit, the values of C_1 and C_2 can be taken from the following equations:

$$\frac{C_1}{C_2} = \sqrt{\frac{r_{be}}{r_a}} \quad (3)$$

$$C_1 \times C_2 = \frac{g'm}{\omega_0^2 R_1'} \quad (4)$$

where:

- r_{be} is the (RF) impedance between base and emitter (of the Darlington)
- r_a is the AC-output impedance (measured at the common emitter)
- g'_m is the transconductance ($= \frac{1}{R_{in}}$ with an emitter follower)
- R_1 is the resonant resistance of the crystal transformed by the load capacitance (see 4.1.2.1., equ. 17)

Figure 6 gives an example of a Pierce oscillator for 1 MHz equipped with a MOSFET (4). A TTL output level is available if the output of the crystal oscillator drives a Schmitt-Trigger (7413). Such an oscillator is suitable for being used as a clock for frequency counters.

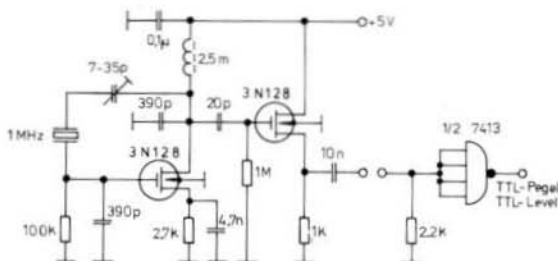


Fig. 6:
Crystal oscillator
equipped with
a MOSFET

1.3. Crystal Oscillators with Overtone AT-Crystals

If a thickness-shear vibrator is excited at an overtone, the crystal disk will oscillate in several subdisks in anti-phase (see illustration at Table 3). Only odd overtones can be excited. The fundamental frequency of an AT-crystal is inversely proportional to the thickness of the disk. For instance, a fundamental crystal for 30 MHz will have a thickness of approximately 55 μm . If this crystal is now excited at the third overtone, e.g. at 90 MHz, the electrical effective sub-disk thickness will be a third, which amounts to approx. 18 μm .

However, the overtone frequency is not exactly a multiple of the fundamental mode frequency; but this so-called anharmonicity will become less and less with the higher order overtones. For this reason, it is relatively simple to operate crystal oscillators even up to frequencies in the order of 300 MHz, although the usual upper frequency limit is 200 MHz/ninth overtone; one can operate the crystal at the eleventh or thirteenth overtone, which is virtually exactly 11/9 or 13/9 times the ninth overtone. However, a crystal with the highest possible fundamental-frequency should be selected (20 MHz to 30 MHz), so that the overtone modes are spaced far from another.

Table 3: Equivalent data of AT-overtone crystals

Over-tone	Frequency range (MHz) for cases			Typical Equivalent Data			
	HC-6/U	HC-25/U	HC-35/HC-45	C_0	C_1	Q	R_1
3	18 - 60 (80)	20 - 60 (90)	27 - 60 (90)	5 - 7 pF [2 - 4 pF]	2 fF [1 fF]	$> 4 \times 10^6$ f (MHz)	20 Ω [40 Ω]
5	40 - 115 (130)	40 - 115 (150)	50 - 125		0.6 - 0.8 fF [0.4 fF]	$> 5 \times 10^6$ f (MHz)	40 Ω [80 Ω]
7	70 - 150	70 - 150	70 - 175		0.3 - 0.4 fF [0.2 fF]		100 Ω [150 Ω]
9	150 - 200	150 - 200	150 - 200		0.2 - 0.3 fF [0.1 fF]		150 Ω [200 Ω]

[] = HC-35/HC-45

The typical equivalent data are given in **Table 3**. The motional capacitance C_1 reduces as a square of the overtone n :

$$C_1 \text{ typ} \sim \frac{1}{n^2} \quad (5)$$

The attainable Q -value will also fall on increasing frequency. For this reason, the R_1 values will increase, and will be in the order of typically 20 to 200 Ω .

On increasing frequency, the static capacitance C_0 will form an ever increasing bypass for the crystal. The results of this can be seen in **Figure 7**. Given is the locus of the complex crystal impedance. In the vicinity of parallel and series resonance, it will represent a circle, which cuts the real axis at f_s and f_p . The spacing of the center point of the circle from the real axis will become greater, the lower the reactive resistance of C_0 . At low values of X_{C_0} , the phase slope in the vicinity of series resonance will be lower, and especially the phase deviation will be less in the inductive direction. Finally, it can happen that the circumference no longer cuts the real axis, which means that no real resonant point is present, at which the crystal is purely ohmic. For this reason, the static capacitance should be compensated for using a parallel inductance:

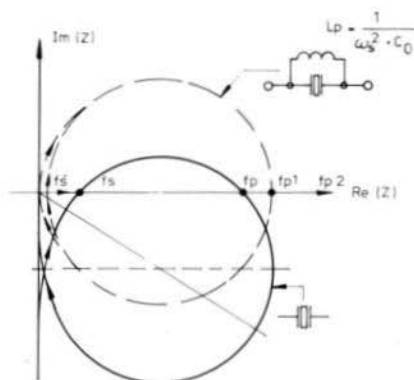
$$L_p = \frac{1}{\omega_s^2 \cdot C_0} \quad (6)$$

in excess of a certain limit.

A rule-of-thumb for this limit is:

C_0 -compensation should be provided when $X_{C_0} < 5 \times R_1$, or generally in excess of 100 MHz.

Fig. 7:
Locus of a crystal
with and without
 C_0 -compensation



The result of the compensation is given in Figure 7 in the form of a dashed line. The locus is symmetric to the real axis, however, there exist two parallel resonances above and below f_s . The attainable total phase deviation is up to $\pm 90^\circ$.

A compensating coil having a low Q ($R_p > 10 R_1$) is suitable, and the compensation condition (6) need not be exactly maintained. It is sufficient to use a standard inductance (or a corresponding number of turns wound on a 10 k Ω resistor).

Aperiodic oscillators will not operate reliably with overtone crystals, even when this is stated from time to time (5). A resonant circuit should always be provided in order to avoid oscillation at the fundamental frequency.

When using a Pierce circuit as shown in Figure 4 b, it is possible for the collector capacitor to be replaced by a capacitively detuned circuit. Since overtone crystals are usually aligned in series resonance, this will result in a residual load capacitance for this circuit, which means that only customer-specified crystals will operate satisfactorily.

In order to pull the crystal frequency towards a lower value, an inductance is often connected in series with the crystal. However, it is possible for parasitic oscillations to be excited across this inductance L and the static capacitance of the crystal C_0 , which could be difficult to neutralize (see section 4).

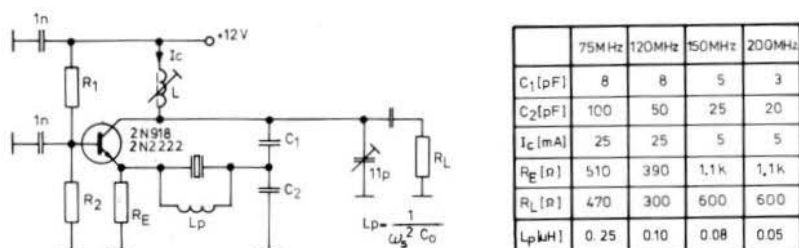


Fig. 8: Overtone crystal oscillator up to 200 MHz

It is therefore better to use a true series-resonant circuit as shown in Figure 8. The values of C_1 and C_2 are selected so that a sufficient loop gain results. This is reduced both by the divider C_1/C_2 and by the voltage division across the crystal impedance and the input impedance at the emitter (20).

When selecting a suitable transistor, a rule-of-thumb is, that the transit frequency should be at least ten times that of the oscillator frequency. In addition to this, transistors are to be recommended that have a high DC-gain (h_{FE}) at a low base resistance (r_{bb}).

2. LOAD CAPACITANCE; OSCILLATORS WITH PARALLEL AND SERIES RESONANCE

The designations series and parallel resonance are often combined in a confusing manner. In the case of series-resonance crystal oscillators, the crystal will oscillate together with its pulling elements at the low-impedance resonance. Such a case is the example of the Butler oscillator given in Figure 3. However, this does not mean that the oscillator operates at the series-resonance frequency of the crystal. The Butler remains a series-resonance oscillator, even when the crystal is pulled with the aid of a series capacitor, or even when (at higher frequencies) the phase angle of the transistor gain deviates from 0° or 180° .

On the other hand, another commonly used definition is not advisable: This states that a series-resonance oscillator is designated by the fact that the oscillator will also oscillate when the crystal is replaced by a resistor. If this were the case, the Butler oscillator given in Figure 3 would not be a series-resonance oscillator; however, would be, if the collector resistor of transistor 1 was replaced by a resonant circuit.

A series load capacitance C_L will generate a new series resonance at

$$f_{CL} = f_s \left(1 + \frac{C_1}{2(C_0 + C_L)} \right) \quad (7)$$

In the case of a parallel-resonance oscillator, the oscillator will operate at a high-impedance resonance together with its adjacent (pulling) elements. In the case of the Colpitts oscillator shown in Figure 5, C_1 and C_2 are connected in series across the crystal. In the case of an ideal amplifier stage they will form the load capacitance C_L and reduce the parallel resonance frequency of the crystal to f_{CL} . If this value of C_L is just as great as the series- C_L in the upper case, the pulled series-resonance frequency will be the same as the pulled parallel-resonance in the last example. In both cases, the crystal will operate at a point at which it behaves as a high-Q inductance. This is summarized in **Figure 9**.

Crystals that are designated with a load capacitance are usually aligned by the manufacturer in conjunction with a series capacitor. However, since both measurements are equivalent, it is immaterial for the crystal specification whether a parallel or series resonance oscillator is to be used. It is sufficient for a load capacitance to be given. In this case it is advisable, if possible, for standard values of C_L (e.g. 30 pF) to be used by varying the other capacitances of the oscillator.

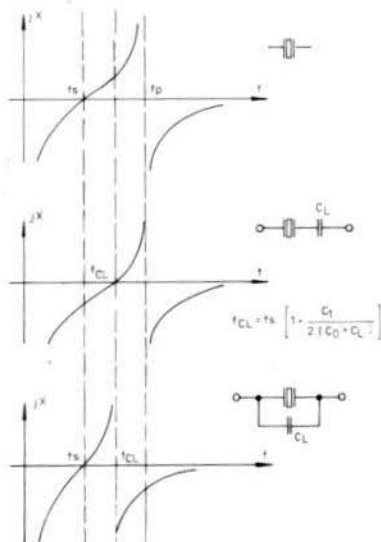


Fig. 9: Crystals with load capacitances

3. CRYSTAL DISSIPATION IN THE OSCILLATOR

3.1. Typical Values

The crystal dissipation of crystals will exhibit the following values in the various oscillator circuits:

Tube oscillator:	1 to 10 mW, typical 2 mW
TTL-oscillator:	1 to 5 mW
Transistor oscillator:	10 μ W to 1 mW, typical 100 μ W
CMOS oscillator:	1 μ W to 100 μ W

Since the crystal frequency and resonance impedance are somewhat dependent on the load, a nominal load should be specified especially for low-tolerance crystals. The following limits are advisable physically:

Crystal Drive Level not more than 2 mW

Higher drive levels will deteriorate the stability, the Q and aging characteristics. In the case of LF-crystals, and very small AT-crystals (cases HC-45/U or HC-35/U), 2 mW will be too much. Since reactive power = Q x effective power, a reactive power of 200 W will be periodically present at the reactances of the crystal at a drive level of 2 mW and a Q of 100 000 !

Crystal Drive Level not less than 1 μ W

Too low a drive level could cause difficulties in commencing oscillation, since – physically speaking – a certain minimum amount of energy is required for commencing oscillation. This varies, as a result of unavoidable fluctuations in the quality of the transition crystal/electrode (in the submicroscopic range), and other damping influences. This can cause problems with certain CMOS and other low-power oscillators.

3.2. Practical Determination of the Crystal Drive Level

Since the transistor parameters are only low-signal magnitudes, they are only valid as long as the transistor operates in class A. In the case of a self-limiting oscillator, the transistor operates up into the non-linear saturation range. Therefore, it is virtually impossible to calculate the expected drive level of the crystal.

In order to determine the actual drive level of the crystal in a measuring setup, either the RF-current to the crystal or the voltage difference across the crystal is measured with the aid of a thermistor, oscilloscope or RF-voltmeter. If the equivalent data of the crystal (C_0 , C_1 , R_1) are known, it is possible for the phase angle to be calculated from the oscillator frequency. Finally, the actual power can be determined from this. This is often very much lower than would result without consideration of the phase.

4. PULLABILITY AND MODULATION OF CRYSTAL OSCILLATORS

4.1. Pullability

The pullability of the oscillator frequency is dependent both on the pulling reactances of the circuit and the equivalent data of the crystal.

4.1.1. Pulling Reactances

The reactive impedance characteristic of a crystal is given in **Figure 10a**, whose frequency is pulled using an inductance, or a series-resonant circuit in series with the crystal. Generally speaking, the series resonance will be pulled to the following with the aid of a connected reactive impedance X_V :

$$f_X \approx f_S \left[1 + \frac{C_1}{2 \left(C_0 - \frac{1}{\omega_S X_V} \right)} \right] \quad (8)$$

A series capacitor C_V will increase the frequency to

$$f_C \approx f_s \left(1 + \frac{C_1}{2(C_0 + C_V)} \right) \quad (9)$$

A series inductance L_V will reduce the frequency to

$$f_{L_1} \approx f_s \left[1 - \frac{C_1}{\left(2 \frac{1}{\omega_s^2 L_V} - C_0 \right)} \right] \quad (10)$$

If a series resonant circuit is connected, it is possible for the series-resonant frequency to be tuned up and down:

$$f_{LC_1} \approx f_s \left[1 + \frac{C_1}{2 \left(C_0 - \frac{1}{\omega_s^2 L_V} - \frac{1}{C_V} \right)} \right] \quad (11)$$

These equations are valid at sufficient accuracy for the pulling range up to 1000 ppm (10^{-3}).

If an inductance is provided as pulling element, an additional series-resonance point (f_{L_2} or f_{LC_2}) will appear. At this position, the connected inductive reactive impedance will be in resonance with the capacitance C_0 of the crystal. This frequency can, it is true, be relatively far from the main resonance, however, it is possible for the oscillator to jump to this parasitic resonance.

The reactance characteristics of the circuit when provided with an additional parallel compensation of C_0 , are given in **Figure 10 b**. This will lead to two parallel resonance positions at

$$f_{p_{1,2}} \approx f_s \left(1 \pm \frac{1}{2} \sqrt{\frac{C_1}{C_0}} \right) \quad (12)$$

which are several hundred kHz below and above the main resonance frequency. The parallel inductance will increase the pulling range and is usually designed so that it is in resonance with the static crystal capacitance C_0 :

$$L_p = \frac{1}{\omega_s^2 C_0} \quad (13)$$

The pulling equations result in the same manner as for equations 8 to 11, however, without the term C_0 . In detail:

A series capacitor C_V will increase the series resonance to

$$f_{C_2} \approx f_s \left(1 + \frac{C_1}{2 C_V} \right) \quad (14)$$

however, an additional series-resonance point f_{C_1} will appear below f_{p_1} .

A series inductance L_V will reduce the main resonance to

$$f_{L_1} \approx f_s \left(1 - \frac{C_1}{2 \omega_s^2 L_V} \right) \quad (15)$$

whereby a further series-resonance position f_{L_2} will appear in excess of f_{p_2} .

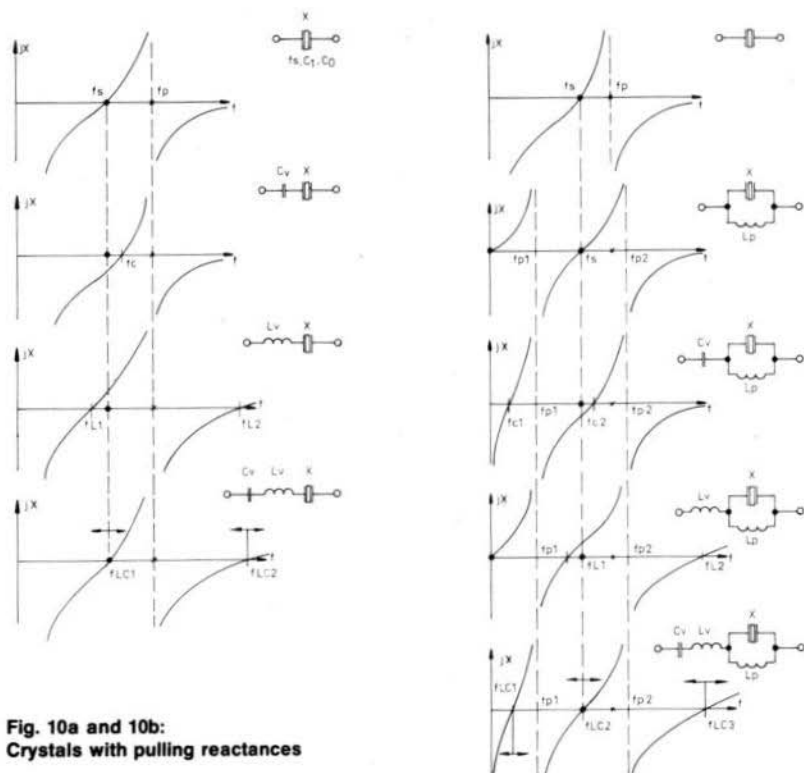


Fig. 10a and 10b:
Crystals with pulling reactances

When pulling the frequency using a series circuit L_V , C_V , a new frequency will result as:

$$f_{LC_2} \approx f_s \left[1 - \frac{C_1}{2} \left(\omega^2 L_V - \frac{1}{C_V} \right) \right] \quad (16)$$

which can be below or above the main resonance.

In this case, two further series resonances f_{LC_1} and f_{LC_3} appear.

All additional resonance points are not crystal-controlled, but are parasitic resonances between the pulling link and the detuned circuit comprising C_0 and L_p , which differs from the main resonance in a capacitive or inductive direction.

In the case of oscillators with a large pulling range, these additional resonances can cause considerable problems in the form of a jumping of the oscillator frequency. Since the parasitic resonances are often of lower impedance than the pulled main resonance, it is often difficult to avoid such jumping of the frequency.

Figure 11 provides a quantitative evaluation of the pulling behaviour of the different types of circuit. It is based on a fundamental-wave crystal of 10 MHz with $C_0 = 6$ pF and $C_1 = 20$ fF with and without C_0 -compensation. A series capacitor is compared to a series-resonant circuit L_V , C_V , when used as pulling element. In this case, C_V was varied between 10 pF and

30 pF, and L_V was selected so that the series-resonant circuit was tuned to the crystal frequency f_s at a mean $\bar{C}_V = \sqrt{10 \times 30 \text{ pF}}$. This resulted in a pulling range that was approximately symmetrically spread around f_s .

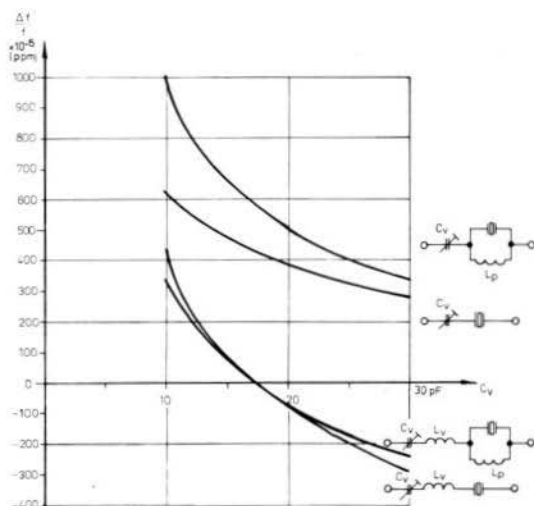


Fig. 11:
Pulling characteristic
of different circuits
with $C_V = 10 - 30 \text{ pF}$.
Parameters: Fundamental mode
AT-crystal with
 $C_0 = 6 \text{ pF}$; $C_1 = 20 \text{ fF}$.

$$L_V = \frac{1}{\omega_s^2 \sqrt{10 \text{ pF} \times 30 \text{ pF}}}$$

$$L_P = \frac{1}{\omega_s^2 C_0}$$

These curves were extended by a complex circuit analysis by which the crystal losses ($Q_Q = 39\,800$) and the coil losses ($Q_{L_V} = Q_{L_P} = 100$) were taken into consideration. The results of this are summarized in **Table 4**.

Pulling range $\frac{\Delta f}{f}$ (ppm)	347	6 622	61 665	61 666
R_1' (10 pF)	51.2 Ω	40.6 Ω	29.6 Ω	30.9 Ω
Impedance transformation R_1' (30 pF)	28.8 Ω	23.8 Ω	21.1 Ω	29.8 Ω
Effective Q	$Q' = 39\,800$	$Q' = 30\,800 - 24\,400$	$Q' = 27\,000 - 37\,700$	$Q' = 26\,000 - 27\,000$

Crystal:
 Fundamental wave-AT, $C_0 = 6 \text{ pF}$; $C_1 = 20 \text{ fF}$; $R_1 = 20 \text{ }\Omega$ ($Q_{QU} = 39\,800$)

Pulling elements: $L_V = \frac{1}{\omega_0^2 \sqrt{10 \text{ pF} \cdot 30 \text{ pF}}}$; $L_P = \frac{1}{\omega_0^2 \cdot C_0}$; $Q_{L_V} = Q_{L_P} = 100$
 (at 10 MHz: $L_V = 14,6 \text{ }\mu\text{H}$; $L_P = 42,2 \text{ }\mu\text{H}$)

Table 4: Pulling behaviour of various types of pulling circuits for $C_V = 10$ to 30 pF

4.1.2. Remarks on the Pulling Circuits

4.1.2.1. Crystal without C_0 -Compensation

If only a pulling capacitor C_V is used, this will result in the smallest pulling range, and all frequencies will be below the crystal frequency. The overall Q will remain practically constant over the whole range (same crystal Q), however, the series-resonance impedance will be transformed up to the following value:

$$R_1' = R_1 \left(1 + \frac{C_0}{C_L}\right)^2 \quad (17)$$

At very low load capacitances, it is possible for R_1' to attain very high values (e.g. at 5 pF, $R_1' = 96.8 \Omega$). This can cause the oscillator to cease operation, or cause problems in commencing oscillation. Since the pullability increases considerably at such low capacitances (see equ. 9), this can cause instability, or non-reproducibility of the oscillator frequency. This fault is often to be found in the data sheets of integrated circuits. For instance, an effective load capacitance of approximately 6 pF (!) is given in the original data sheet of the well-known mixer SO 42 P. Similar load values are given in conjunction with the μ P-clock oscillator of the 8080-system.

In a series circuit, the pulling range will be considerably larger and can be set to be symmetrical to the crystal series resonance. The transformed impedance is less than in the first case. The overall Q will, however, deteriorate greatly due to the inductance. As can be seen in **Figure 12**, it is possible for the pulling range to be greatly extended asymmetrically towards lower frequencies, if L_V is increased, however, the overall Q will quickly disappear. It will be seen in the lower curve of Figure 12 that the pulling range is 1106×10^{-6} , however, the Q is reduced to 12 500! This is a general rule for any pulling circuit equipped with inductances.

4.1.2.2. Crystals with C_0 -Compensation

The pulling range will be very large if only one pulling capacitor is used in addition to the C_0 -compensation, and the transformed dissipation resistance R_1' will be considerably more favorable than with other circuits. The overall Q also remains relatively high. It is only of disadvantage for certain applications that the oscillator frequency will always be in excess of the crystal frequency.

When using a series-circuit in addition to the C_0 -compensation, the pulling range will not be larger than in the previous example in spite of the larger number of components; however, it will be symmetric to the crystal frequency. It is true that R_1' is relatively constant, however, the overall Q is very low due to the two inductances.

To summarize, it should be noted that larger pulling ranges are possible with C_0 -compensation than without. However, the effect of the compensation is reduced to a minimum when pulling with a series-resonant circuit. In order to achieve a large pulling range, it is usually best to use a circuit with C_0 -compensation and pulling capacitor (upper curve in Figure 11).

4.1.3. Effect of the Motional Parameters of the Crystal

As can be seen in equations (8) to (16), the pullability will be better, the greater the dynamic capacitance C_1 of the crystal. This can be influenced within certain limits by the design of the crystal, however, this will cause an increase of the static capacitance C_0 of the crystal, as well as an increase of the intensity of unwanted, anharmonic modes. For this reason, the realization of extreme pulling demands in practice should be found in close cooperation with the crystal manufacturer.

The pullability of overtone crystals is reduced by factor $1/n^2$ in the same manner as the motional capacitance C_1 . **Table 5** gives the values for the simplest pulling circuit using only a pulling capacitor without C_0 -compensation. A crystal oscillator of an oscillator chain which is to be pulled in frequency should therefore be equipped with a crystal having a high fundamental-wave frequency (20 to 30 MHz), whereas the lowest possible overtone should be used in the case of overtone crystals.


					
$C_{\text{series}} = 10 - 30 \text{ pF}$	Funda- (mental)	3rd overtone ₁	5th overtone ₁	7th overtone ₁	9th overtone ₁
Crystal data: C_0	6 pF	5 pF	5 pF	5 pF	5 pF
C_1	20 fF	2 fF	0.7 fF	0.35 fF	0.25 fF
Pulling range $\frac{\Delta f}{f}$	$347 \cdot 10^{-6}$	$38.1 \cdot 10^{-6}$	$13.3 \cdot 10^{-6}$	$6.7 \cdot 10^{-6}$	$4.7 \cdot 10^{-6}$

Table 5: Pullability as a function of overtone

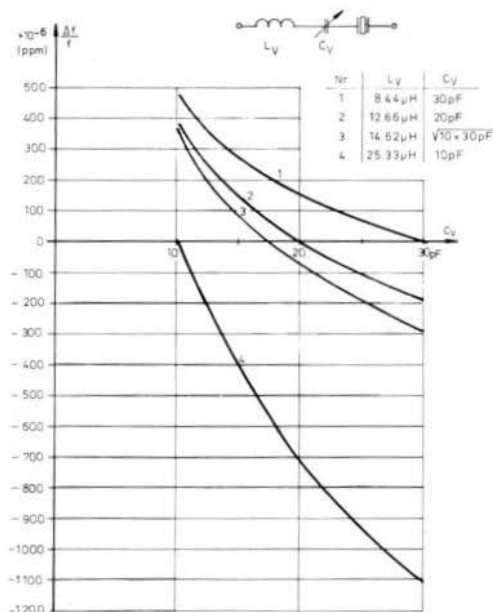


Fig. 12:
Pulling with series-resonance circuits
 $C_v = 10 - 30 \text{ pF}$
Parameter:
 $C_0 = 6 \text{ pF}$
 $C_1 = 20 \text{ fF}$

4.2. Modulation of Crystal Oscillators

The pulling curves given in **Figures 11 and 12** are more or less non-linear. When pulling with varactor diodes, the non-linearity of the capacitance-voltage characteristic will have an opposite effect, which means that this will improve the modulation characteristic.

As an example, the modulation characteristic is given in **Figure 13** when using a varactor diode type BB 109 in conjunction with the four pulling circuits given in section 4.1.

The capacitance-voltage characteristic of the diode is given in **Figure 13a**.

Even the simplest pulling circuit results in a practically straight modulation characteristic in this (special) case. Even the circuit equipped with a series-circuit will provide good linearity. On the other hand, the C_0 -compensated pulling circuit will be inferior to the appropriate uncompensated circuit – especially at larger frequency-deviation levels.

It is assumed during this calculation that the RF-voltage across the varactor diode is considerably less than the DC-voltage, which is usually not the case. This is to be shown in **Figure 14** as an example using the simplest pulling circuit. At resonance, the crystal will possess an inductive reactive impedance that coincides with the reactive impedance of the load capacitance of the opposite sign. C_0 is not taken into consideration here. If the total voltage U_0 is present across the crystal and varactor diode, the following voltage values will be present across the reactance of the crystal and the load capacitance, which is assumed to be loss-less:

$$U_{L_1} = U_{C_D} = Q_q \times U_0 \quad (18)$$

where Q_q is the Q of the crystal. The voltage U_0 is present across R_1 and will determine the drive level of the crystal. At a drive level of P_{q_1} , a voltage will be built up across the varactor diode due to the resonance peak.

$$U_{C_D} = Q_q \sqrt{P_{q_1} \cdot R_1} = \frac{1}{\omega_0 C_1} \sqrt{\frac{P_{q_1}}{R_1}} \quad (19)$$

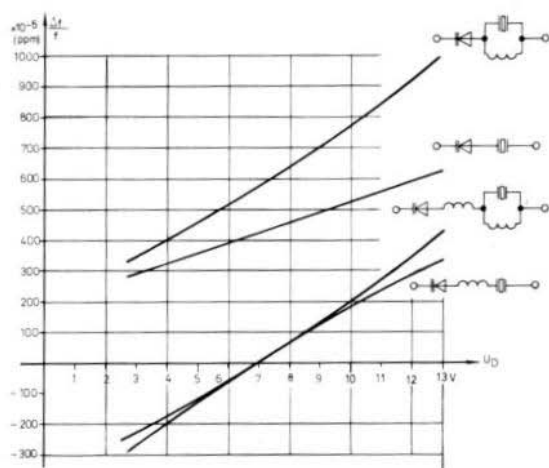


Fig. 13:
Modulation behaviour
with varactor diodes
BB 109

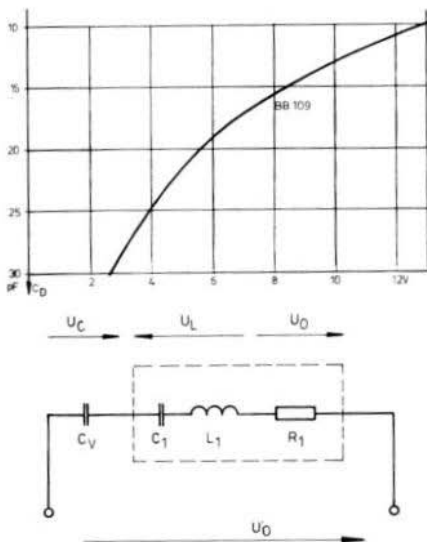


Fig. 13a:
Diode characteristic
 $C_D = f(U_D)$

Fig. 14:
Resonance peak
across the load
capacitance

Example: $P_q = 2 \text{ mW}$, $R_1 = 20 \Omega$, $f_0 = 10 \text{ MHz}$, $C_D = 10 \text{ pF}$

In this realistic case, an AC-voltage will result across the varactor diode of $U_{C_D} = 15.9 \text{ V}$, which corresponds to a peak-to-peak voltage of 45 V, which is superimposed on the DC-voltage. In the case of the diode BB 109, a bias voltage of approximately 13 V is necessary for $C_D = 10 \text{ pF}$. Even then, the whole diode characteristic will be swept in time with the RF-voltage! This will be improved by the anti-phase (series) connection of two diodes, but will always be problematic!

REFERENCES for Part 1

- (1) Telefunken Laborbuch Band 3, page 272; Ulm 1968
- (2) Kristallverarbeitung Neckarbischofsheim, catalogue 1976, page 14
- (3) L. Omlin: Analyse und Dimensionierung von Quarzoszillatoren
Elektroniker-Hefte 6, 9, 12 (1977)
- (4) R. Harrison, VK 2 ZTB: Survey of crystal oscillators
HAM RADIO 3/1976, page 10
- (5) C. Hall, WA 5 SNZ: Overtone crystal oscillators without inductors
HAM RADIO 4/1978, page 50

The concluding second part will feature:

5. Frequency stability of crystal oscillators
6. Diode switching of several crystals
7. Modern crystal oscillators using ICs

EDITORIAL NOTES

AN SSB TRANSMITTER FOR THE 13 cm BAND – by R. Galle, VK 5 QR

Edition 2/1979, pages 76-84

A group of West-Australian amateurs are building several versions of this transmitter for 1296 MHz. However, the main interest seems to be for transmitters for the higher GHz bands. The author has constructed a further two processors in order to operate on the 9 cm band: One divides by eight and the other by nine. The divide-by-nine unit operates using two divide-by-three modules in series. The input of this processor has been designed for 30 MHz, with down-conversion to 28 MHz. An experiment made to divide 21 MHz by 9 was not successful since the converted frequencies were so close together that selectivity was very difficult.

The last varactor tripler is also equipped with a varactor VSE 66 P (Mullard/Philips) and is similar to that described for 2304 MHz. It offers approximately 1 W output at 3456 MHz. A 2 m diameter dish produces a considerable signal, but the beamwidth is too narrow. The author recommends a 1 m dish. A trapezoidal log. periodic antenna is used for feeding the dish, as was described in the Radio Communication Handbook. This allows the author to operate on 9 cm, 13 cm, and 23 cm using a single feed and cable. The converters and varactor multipliers are switched to the antenna in the shack. The processor equipped with the divide-by-eight module requires a quadrupler of 432 to 1728 MHz, and a doubler to 3456 MHz.

AF-CIRCUITS OF THE FM RECEIVER – DK 1 OF 035

Edition 1/1979, pages 44-53

Two incorrect capacitance values are given for the lowpass filter: the two capacitors between the 68 k Ω resistors must be 1 nF, and not 10 nF. In addition to this, the feedback capacitor of the TDA 1037 should also be 1 nF in the component location plan given in Figure 9.

SYNTHESIZER FOR THE 2 m BAND – DC 1 QW 001

Edition 3/1978, pages 130-144

If the two crystals Q 1 and Q 2 do not commence oscillation, the following is recommended:

Increase the value of the emitter capacitor of T 9 from 15 to 30 pF; the pulling capacitors (22 pF) should then be fully inserted. It will be possible to switch both crystals at a certain tuning of L 1.

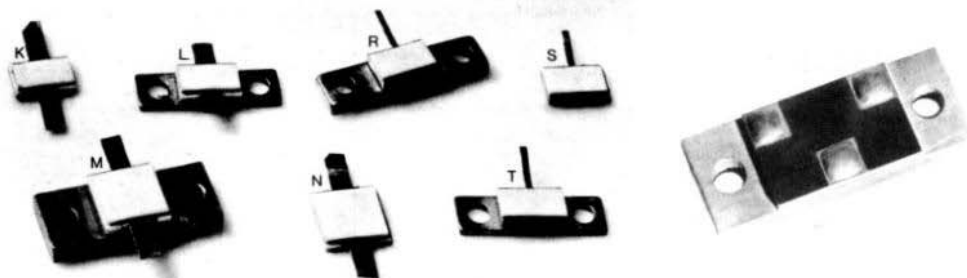
AF-AMPLIFIER OF THE FM-TRANSMITTER – DK 1 OF 037

Edition 2/1979, pages 103-113

The value of C 13 is given correctly in the circuit diagram (Figure 17): 0.1 μ F. The value given in the component location plan (Figure 18) is not correct.

Terminating Resistors for Stripline Application

Although not new in professional circles, resistors for attenuators and terminations in stripline technology are still not well known to radio amateurs. Such stripline resistors can be used up to several GHz. Resistors suitable for attenuators are provided with two connections (type K, L, M) and values of 50 or 100 Ω (CTC), or between 10 Ω and 250 Ω (EMC).



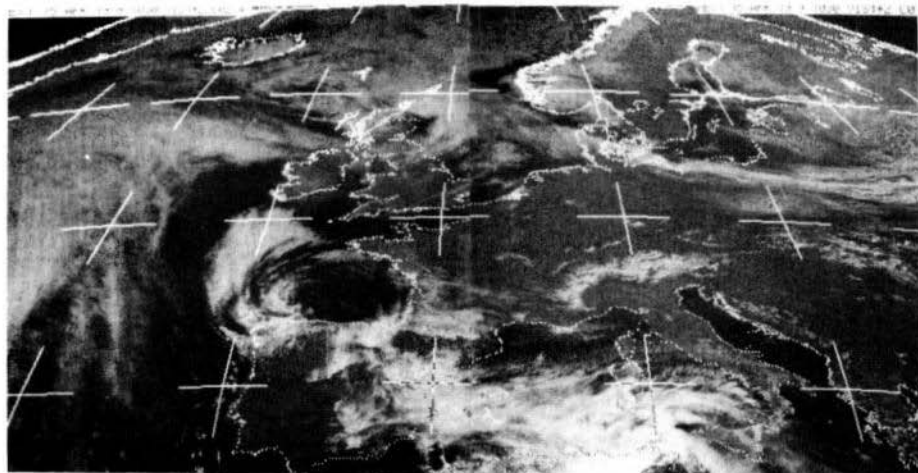
Terminating resistors only have one stripline connection (R, S, T) and a resistance value of 50 Ω . All types can be used for DC up to at least 1 GHz, and special versions can be used up to 2 GHz and even up to 4 GHz. Both capsuled versions with or without bolts as well as chips are available.

Of course, only a few types have been mentioned out of the wide range, and further details can be obtained from the manufacturers.

MATERIAL PRICE LIST OF EQUIPMENT described in Edition 3/1979 of VHF COMMUNICATIONS

DJ 8 IL	20 W POWER AMPLIFIER for 2 m	Ed. 3/1979
PC-board	DJ 8 IL 003 with thru-contacts	DM 15.—
Semiconductors	DJ 8 IL 003 1 pc. BGY 36, 6 diodes	DM 183.—
Minikit	DJ 8 IL 003 1 pl. foil trimmer, 2 tantalum electrolytic, 13 ceram.caps., 4 resistors, 1 heat sink, 2 BNC conn. 105 cm RG-174/U	DM 34.—
Kit	DJ 8 IL 003 complete with above parts	DM 230.—
DC 3 NT	1.2 m PARABOLIC DISH KIT	Ed. 3/1979
Kit	Parabolic dish comprising 12 segments and centre disc. All holes drilled. Aluminium plate 1 mm thick. Including mounting hardware for radiator. Without rivets and riveting machine.	DM 295.—
	Rear mount	DM 60.—
Radiator	Ready-to-operate with screws for mounting to parabolic dish	
	For 24 cm band	DM 150.—
	For METEOSAT (1693 MHz)	DM 135.—
	For 13 cm band	DM 145.—
	Riveting machine for use with hollow rivets upto 5 mm dia. also suitable for other applications	DM 75.—
Hollow rivets	250 pcs. aluminium 3 x 5.5 mm	DM 15.—
	Complete parabolic antenna for above frequencies 1.2 m diameter. Assembled and ready-to-operate with rear mount	DM 725.—

COMPLETE RECEIVE AND IMAGE PROCESSING SYSTEMS FOR THE METEOSAT AND GOES SATELLITES



We are now able to offer a complete METEOSAT APT Reception System for professional users. This compact, inexpensive system includes the following modules:

- 1.2 m parabolic dish complete with radiator
- SHF-Converter in weather-proof casing with noise figure ≤ 3 dB
- VHF-Receiver, especially designed for METEOSAT reception
- APT Image-processing system with either Polaroid camera system or FAX-recording.

Details on METEOSAT reception were given in edition 3/78, 4/78, and 3/79 of VHF COMMUNICATIONS. The basic principle of operation of the two types of image processing were also explained in these editions.

Further details and offers on request.

UKW - TECHNIK · Hans Dohlus oHG
D-8523 BAIERSDORF · Jahnstraße 14
Telephone (09133) - 855, 856 · Telex: 629 887

Bank accounts: Postscheck Nürnberg 30 455 - 858

Space and Astronomical Slides

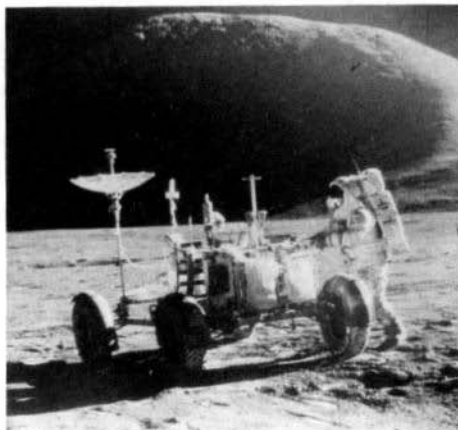
Informative and Impressive

VHF COMMUNICATIONS now offers sets of fantastic slides made during the Gemini, Apollo, Mariner, and Voyager missions, as well as slides from leading observatories. These are standard size 5 cm x 5 cm slides which are framed and annotated.

Prices plus DM 3.00 for post and packing.

Sets of 5 NASA-slides DM 8.50 per set

Set 8103	Apollo 11: Earth and Moon
Set 8104	Apollo 11: Man of the Moon
Set 8105	Apollo 9 and 10: Moon Rehearsal
Set 8106	From California to Cap Canaveral
Set 8107	Apollo 12: Moon Revisited
Set 8108	Gemini Earth Views
Set 8109	Apollo 15: Roving Hadley Rille
Set 8110	Apollo 16: Into the Highlands
Set 8111	Apollo 17: Last voyage to the moon
Set 8112	Apollo 17: Last Moon Walks
Set 8113	Mariner 10: Mercury and Venus



Set 8147 »Jupiter encountered« 20 slides of VOYAGER 1 & 2 DM 35.00

1. Jupiter and 3 satellites 2. The giant planet 3. Jupiter, Io and Europa 4. The Red spot 5. The Red spot in detail 6. The swirling clouds 7. Io and a white oval 8. The neighbourhood of the Red spot 9. The rings of Jupiter 10. The Galilean satellites 11. Amalthea 12. Callisto 13. Impact feature on Callisto 14. Eruption on Io 15. Io full disc 16. Europa close-up 17. Europa distant view 18. Ganymede close-up 19. A distant Ganymede 20. The jovian system

Set 8100 »Saturn encountered«, 20 VOYAGER-1 slides DM 35.00

1. Saturn and 6 of its moons 2. Saturn from 11 mio miles 3. Saturn from 8 mio miles 4. Saturn from 1 mio miles 5. Saturn and rings from 900.000 miles 6. Saturn's Red spot 7. Cloud belts in detail 8. Dions against Saturn 9. Dione close-up 10. Rhea 11. Craters of Rhea 12. Titan 13. Titan's polar hood 14. Huge crater on Mimas 15. Other side of Mimas 16. Approaching the rings 17. Under the rings 18. Below the rings 19. «Braided» F ring 20. Iapetus

Set 8148 »VOYAGER 2 at Saturn«, 20 VOYAGER-2 slides DM 35.00

1. VOYAGER 2 approaches 2. Clouds & rings 3. Storms & satellites 4. Cyclones, spots & jet streams 5. Convective regions 6. Atmospheric disturbance 7. Rings & shadows 8. The «C» ring 9. Ring details 10. The «A» ring 11. Looking back on Saturn 12. Titan - night side 13. Titan - atmospheric bands 14. The «F» ring 15. Hyperion close-up 16. Iapetus revealed 17. Enceladus explored 18. The Tethys canyon 19. The «F» ring structure 20. Within the Enke division

Set 8102 »The Solar System«, 20 NASA/JPL slides DM 35.00

1. Solar System 2. Formation of the Planets 3. The Sun 4. Mercury 5. Crescent Venus 6. Clouds of Venus 7. Earth 8. Full Moon 9. Mars 10. Mars: Olympus Mons 11. Mars: Grand Canyon 12. Mars: Sinuous Channel 13. Phobos 14. Jupiter with Moons 15. Jupiter Red Spot 16. Saturn 17. Saturn Rings 18. Uranus and Neptune 19. Pluto 20. Comet Ikeya-Seki.

Set 8149 »The Sun in action«, 20 NASA/JPL slides DM 35.00

1. Sun in H α light 2. Total Solar eclipse 3. Outer corona 4. Corona from SMM satellite 5. Corona close-up 6. Solar magnetogram 7. Active regions in X-radiation 8. X-ray corona 9. A coronal hole 10. Solar flare 11. Active Sun 12. Eruptive prominence 13. Gargantuan prominence 14. Eruptive prominence 15. Huge Solar explosion 16. Prominence in action 17. Sun in action 18. Magnetic field loops 19. Prominence close-up 20. Chromospheric spray

Set 8144 »Space shuttle«, 12 first-flight slides DM 24.00

1. STS1 heads aloft 2. View from the tower 3. Tower clear 4. Launch profile 5. Payload bay open 6. STS control Houston 7. In orbit, earth seen through the windows 8. Bob Crippen in mid-deck 9. John Young 10. Approaching touchdown 11. After 54.5 hours in space Columbia returns to Earth. 12. Astronauts Crippen and Young emerge after the successful mission

Set 8150 »Stars and Galaxies«, 30 astro color slides, AAT 1977 - 1982, DM 46.00

1. The Anglo-Australian 3.9 m Telescope (AAT) 2. AAT Dome 3. Telescope Control Console 4. An Observer at the Prime Focus 5. Star Trails in the SW 6. Circumpolar Star Trails 7. Centaurus A. NGC 5128 8. The Spiral Galaxy M83 (NGC 5236) 9. The Eta Carinae Nebula 10. An open Cluster of Stars NGC 3293 11. A Planetary Nebula. NGC 6302 12. The Trifid Nebula M20 (NGC 6514) 13. The Cone Nebula 14. S Monocerotis and NGC 2264 15. The Helix Nebula. NGC 7293 16. A Wolf-Rayet Star in NGC 2359 17. A Spiral Galaxy. NGC 2997 18. Messier 16 (NGC 6611) 19. The Orion Nebula 20. Dust and Gas in Sagittarius. NGC 6589-90 21. NGC 6164/5, The Nebulosity Around HD 148937 22. Dust Cloud and Open Cluster NGC 6520 23. The Spiral Galaxy NGC 253 24. A Mass-Loss Star. IC 2220 25. The Jewel Box NGC 4755 26. Local Group Galaxy NGC 6822 27. Central Regions of NGC 5128 28. Towards the Galactic Centre 29. The Trapezium 30. The Trifid Stars



UKWberichte Terry D. Bittan · Jahnstr. 14 · Postfach 80 · D-8523 Baiersdorf

Tel. West Germany 9133-855. For Representatives see cover page 2



CRYSTAL FILTERS OSCILLATOR CRYSTALS
**SYNONYMOUS FOR QUALITY
AND ADVANCED TECHNOLOGY**

NEW STANDARD FILTERS

CW-FILTER XF-9NB see table

SWITCHABLE SSB FILTERS

for a fixed carrier frequency of 9.000 MHz

XF-9B 01

8998.5 kHz for LSB

XF-9B 02

9001.5 kHz for USB

See XF-9B for all other specifications
The carrier crystal XF 900 is provided

Filter Type	XF-9A	XF-9B	XF-9C	XF-9D	XF-9E	XF-9NB	
Application	SSB Transmit	SSB	AM	AM	FM	CW	
Number of crystals	5	8	8	8	8	8	
3 dB bandwidth	2.4 kHz	2.3 kHz	3.6 kHz	4.8 kHz	11.5 kHz	0.4 kHz	
6 dB bandwidth	2.5 kHz	2.4 kHz	3.75 kHz	5.0 kHz	12.0 kHz	0.5 kHz	
Ripple	< 1 dB	< 2 dB	< 2 dB	< 2 dB	< 2 dB	< 0.5 dB	
Insertion loss	< 3 dB	< 3.5 dB	< 3.5 dB	< 3.5 dB	< 3.5 dB	< 6.5 dB	
Termination	Z_1	500 Ω	500 Ω	500 Ω	500 Ω	1200 Ω	500 Ω
	C_1	30 pF	30 pF	30 pF	30 pF	30 pF	30 pF
Shape factor	(6.50 dB) 1.7	(6.60 dB) 1.8	(6.60 dB) 1.8	(6.60 dB) 1.8	(6.60 dB) 1.8	(6.60 dB) 2.2	
		(6.80 dB) 2.2	(6.80 dB) 2.2	(6.80 dB) 2.2	(6.80 dB) 2.2	(6.80 dB) 4.0	
Ultimate rejection	> 45 dB	> 100 dB	> 100 dB	> 100 dB	> 90 dB	> 90 dB	

XF-9A and XF-9B complete with XF 901, XF 902
XF-9NB complete with XF 903

KRISTALLVERARBEITUNG NECKARBISCHOFSHHEIM GMBH
D 6924 Neckarbischofsheim · Postfach 7

